MISSOURI S&T

CENTER FOR TRANSPORTATION INFRASTRUCTURE AND SAFETY

Environmental, Mechanical And Life-Cycle Cost Analysis of Bridge Columns

by

Song Wang, Graduate Student[1]
Mohamed Elgawady. Ph.D. [1]
Pramen P. Shrestha, Ph.D., P. E., Associate Professor[2]
Aly Said, Ph.D., P.E., Associate Professor[2]
Dinesh Dhakal, Graduate Student[2]

[1]Missouri University of Science and Technology
[2]University of Nevada, Las Vegas

August 2014

A National University Transportation Center at Missouri University of Science and Technology

Disclaimer

The contents of this report reflect the views of the author(s), who are responsible for the facts and the accuracy of information presented herein. This document is disseminated under the sponsorship of the Department of Transportation, University Transportation Centers Program and the Center for Transportation Infrastructure and Safety NUTC program at the Missouri University of Science and Technology, in the interest of information exchange. The U.S. Government and Center for Transportation Infrastructure and Safety assumes no liability for the contents or use thereof.

Technical Report Documentation Page

1. Report No.	2. Government Accession No.	3. Recipient's Catalog No.
NUTC R337		

4. Title and Subtitle	5. Report Date
Environmental, Mechanical And Life-Cycle Cost Analysis Of Bridge Columns	August 2014
	6. Performing Organization Code

7. Author/s	8. Performing Organization Report No.
Song Wang, Mohamed Elgawady, Pramen P. Shrestha, Aly Said, Dinesh Dhakal	Project #00042499

9. Performing Organization Name and Address	10. Work Unit No. (TRAIS)
Center for Transportation Infrastructure and Safety/NUTC program Missouri University of Science and Technology 220 Engineering Research Lab Rolla, MO 65409	11. Contract or Grant No. DTRT06-G-0014

12. Sponsoring Organization Name and Address	13. Type of Report and Period Covered
U.S. Department of Transportation Research and Innovative Technology Administration 1200 New Jersey Avenue, SE Washington, DC 20590	Final
	14. Sponsoring Agency Code

15. Supplementary Notes

16. Abstract

Corrosion of RC bridge element is one of the major deterioration distresses in US Highway Bridges. FRP composites jackets can be the economic and effective corrosion repair in future, though its practices and field installation as a means of corrosion repair are limited due to limited durability studies. However, in many laboratory tests and some field test, the externally bonded FRP composites shown to have corrosion control properties in chloride laden environment.

In the study, concrete encased in FRP jackets and steel-concrete-FRP columns were subjected to severe environmental cycles. The behavior of the conditioned cylinders was tested under axial cyclic loads. Moreover, the FRP composites jackets are considered as a corrosion repair material for corroded RC bridge pier column and a life-cycle cost analysis procedure is proposed based on the probabilistic model. The use of this probabilistic model needs corrosion parameters, FRP composites durability properties as a statistically distributed random variable input in Monte-Carlo Simulation. The life-cycle cost includes the agency related cost of inspection, maintenance, repair, rehabilitation, cost of failure represented as probability of failure of repaired column, and users cost.

17. Key Words	18. Distribution Statement
Seismic, Durability, Concrete	No restrictions. This document is available to the public through the National Technical Information Service, Springfield, Virginia 22161.

19. Security Classification (of this report)	20. Security Classification (of this page)	21. No. Of Pages	22. Price
unclassified	unclassified	75	

Form DOT F 1700.7 (8-72)

Executive Summary

Corrosion of RC bridge element is one of the major deterioration distresses in US Highway Bridges. FRP composites jackets can be the economic and effective corrosion repair in future, though its practices and field installation as a means of corrosion repair are limited due to limited durability studies. However, in many laboratory tests and some field test, the externally bonded FRP composites shown to have corrosion control properties in chloride laden environment.

In the study, concrete encased in FRP jackets and steel-concrete-FRP columns were subjected to severe environmental cycles. The behavior of the conditioned cylinders was tested under axial cyclic loads. Moreover, the FRP composites jackets are considered as a corrosion repair material for corroded RC bridge pier column and a life-cycle cost analysis procedure is proposed based on the probabilistic model. The use of this probabilistic model needs corrosion parameters, FRP composites durability properties as a statistically distributed random variable input in Monte-Carlo Simulation. The life-cycle cost includes the agency related cost of inspection, maintenance, repair, rehabilitation, cost of failure represented as probability of failure of repaired column, and users cost.

Abbreviations

AADT	Average annual daily traffic
ACI	American concrete institute
BCR	Benefit-cost-ratio
BLCCA	Bridge life cycle cost analysis
CFRP	Carbon fiber reinforced polymer
DOT	Department of transportation
DR	Discount rate
ENR	Engineering news record
EUAC	Equivalent uniform annual cost
FRP	Fiber reinforced polymer
GFRP	Glass fiber reinforced polymer
IRR	Internal rate of return
LCC	Life-cycle cost
LCCA	Life-cycle cost analysis
LRFD	Load resistance factor design
MR&R	Maintenance, repair, and rehabilitation
NBI	National bridge inventory
NCHRP	National cooperative highway research program

NPV	Net present value
PV	Present value
RC	Reinforced concrete
TLCC	Total life-cycle cost
Sq.ft.	Square feet

Table of Content

1 INTRODUCTION

Typical deterioration of concrete structures in marine environments is chloride-induced corrosion of rebar. When a reinforcing steel bar corrodes in concrete, a surface layer of steel is consumed and a layer of corrosion products (rust) forms on the perimeter of the bar. The rust that forms occupies a larger volume than the consumed steel layer, the increased volume creates internal high pressure against the surrounding concrete, and cracking and spalling result. Thus, steel corrosion may cause damage in steel, concrete, and the bond between them.

A concrete cover usually protects reinforcing steel bars in concrete. A sound concrete cover physically provides a direct barrier preventing chemicals chloride ions, carbon dioxide, and so on from approaching the surface of the steel bar. In addition, high alkalinity in concrete chemically protects the embedded bar against corrosion. In typical concrete environments, the pH ranges between 12.5 and 13.5. This produces a film of gama-ferric oxide, or lepidocrite on the bar surface, which acts as a barrier against corrosion, and the steel exists in a passive condition. In a marine environment, however, chloride ions from seawater accumulate on the surface of the concrete and slowly migrate through the concrete cover to the underlying bar. When the chloride ion concentration at the bar depth exceeds a critical threshold value, the protective passive layer on the bar surface breaks down and active steel corrosion begins.

The deterioration progress can be roughly divided into three stages: corrosion initiation stage, corrosion propagation stage and residual life stage. The durability model is shown below.

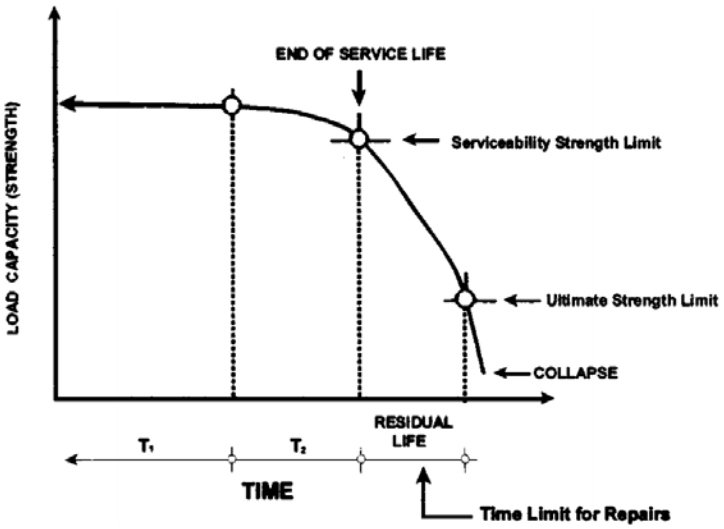

The first phase (corrosion initiation) is from the time of construction to the time of initiation of corrosion. The second phase (corrosion propagation) follows until the first crack appears at the concrete surface. The third phase (residual life) starts from the time of external visual crack until the element reaches the ultimate strength limit and will collapse. The first two stages are most important to service lift of the reinforced concrete structures in marine environment and will be discussed in details below.

1.1 Initiation Stage

The length of corrosion initiation stage is the time for chloride ions from external source (marine environment or deicing salt media) to diffuse into concrete structure at various depths and reach a threshold concentration value. Chloride threshold of rebar in concrete can be defined as the content of chloride at the depth of the rebar that is necessary to sustain localized breakdown of its passive film and hence initiate its active corrosion.

Based on Fick's second law, chloride concentrations for various concrete cover depths at different exposure time intervals can be expressed as below:

$$\frac{\partial C}{\partial t} = D_c \frac{\partial^2 C}{\partial x^2} \qquad (1)$$

Where C is the concentration ($mol \cdot m^{-3}$); t is the time (s); D_c is the chloride diffusion coefficient ($m^2 s^{-1}$) and x is the position (m). In most work, the length of the corrosion initiation stage is approximated with two assumptions:

1) Chloride ions progress inward from the external surface of the concrete, which is covered by aqueous solutions of chlorides. Therefore, the surface chloride concentration remains constant;

2) Chloride ions progress inward by simple diffusion, driven by the gradient of the concentration of chloride ions in the concrete. The effective diffusion coefficient is constant with time and space, and is a property of the concrete between the concrete surface and the steel rebar.

Based on these assumptions, an analytical solution exists to predict the spatial and temporal evolution of chloride concentration profiles in concrete, which is given by

$$C_t = C_s \left[1 - erf\left(\frac{x}{2\sqrt{D_c t}}\right) \right] \qquad (2)$$

where x is the concrete cover depth; C_t is the chloride concentration at cover depth; C_s is the surface chloride concentration; t is time; D_c is the effective diffusion coefficient in concrete; erf is the Gaussian error function as below:

$$erf(z) = \frac{2}{\sqrt{\pi}} \int_0^z e^{-t^2} dt \qquad (3)$$

The effective diffusion coefficient of chloride in water-saturated concrete can be calculated by the following equation:

$$D_c = \frac{1 - V_a}{1 + V_a} D_p \qquad (4)$$

where D_p is the chloride ion diffusion coefficients in the cement paste and V_a is the aggregate volume fraction.

Take the concrete mix proportion from Krk Bridge (I. Stipanovic Oslakovic et al. 2010) as an example to calculate D_c. The mix proportion is listed in the table below:

Table 1 Concrete mix design

Material	Comment	kg per 1 m^3
Cement (w/c = 0.36)	Blast furnace slag cement with 20% of slag (CEM II/A-S 42,5)	450
Water	Potable water	162
Aggregate (0–16 mm)	Alluvial crashed carbonate gravel	1869
Air-entrainer (Pumpcrete N)	0.15% by weight of cement	0.667
Superplasticizer (Fluidal VX-OC)	0.20% by weight of cement	0.890

Based on specific gravity for cement and aggregate is approximately 3.15 and 2.63, respectively, it can be calculated that V_a=0.7 and D_p=4e-12 m^2s^{-1} from M. Castellote, 2001. Therefore, effective diffusion coefficient of chloride is D_c=7.06e-13 m^2s^{-1}.

The surface chloride concentration is the typical chloride concentration in seawater, which is about C_s=19.885 $kg \cdot m^{-3}$.

The typical chloride concentration threshold value can be determined from the report by Browne et al. 1980 and shown in the table below. Federal Highway Administration (FHWA) also report to use 0.3% by mass of binder as the threshold value (Report No. FHWA RD 98 153,

1998). In most cases, engineers adopt the value range from 0.3% to 0.6%. In this study, 0.4% by mass of cement will be adopted.

Table 4 Risk of corrosion initiation depending on the total chloride content [1]

Cl^- % by mass of cement	Cl^- % by mass of concrete for 450 kg cement/m^3	Risk of corrosion
>2.0	>0.37	Certain
1.0–2.0	0.19–0.37	Probable
0.4–1.0	0.08–0.19	Possible
<0.4	<0.08	Negligible

Given the parameters above and chloride concentration threshold value, the chloride concentration by time for certain concrete cover depth can be plotted and are shown here for depth 25mm, 50mm, 75mm, 100mm.

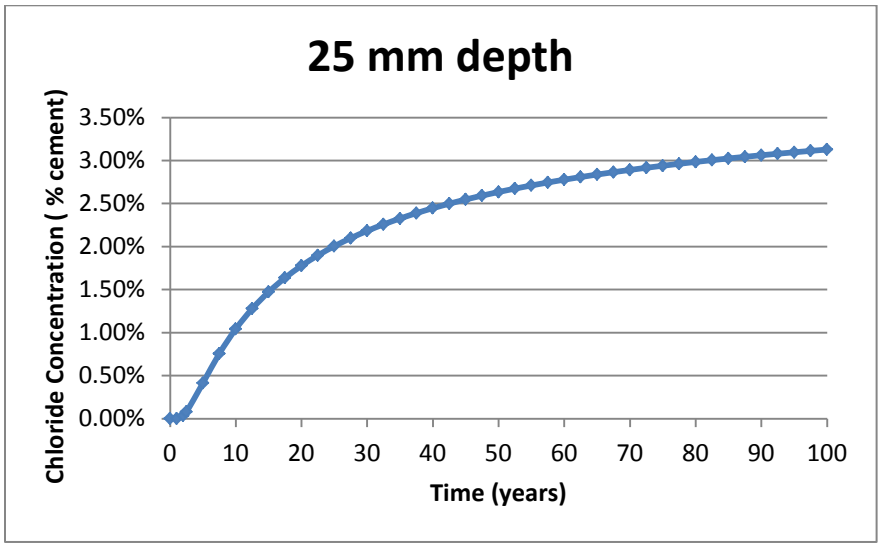

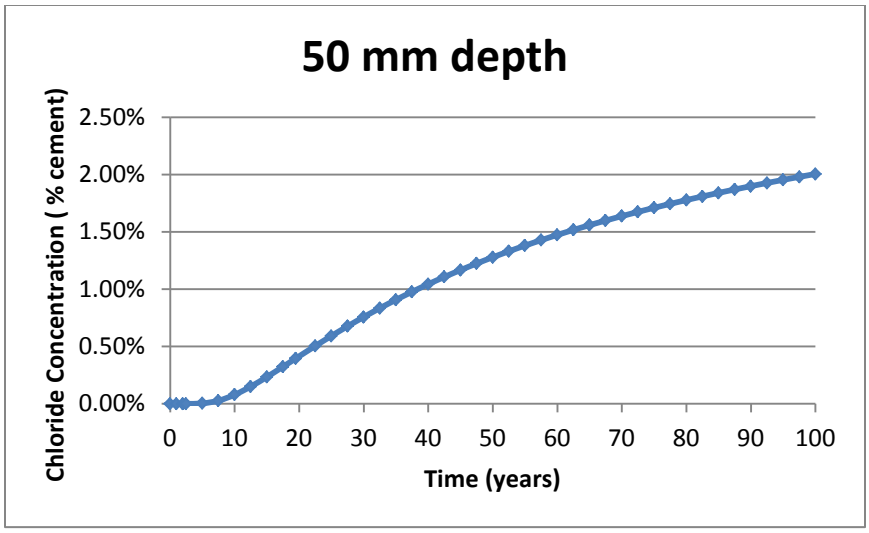
50 mm depth
Chloride Concentration (% cement)
2.50%
2.00%
1.50%
1.00%
0.50%
0.00%
0
10
20
30
40
50
60
70
80
90
100
Time (years)

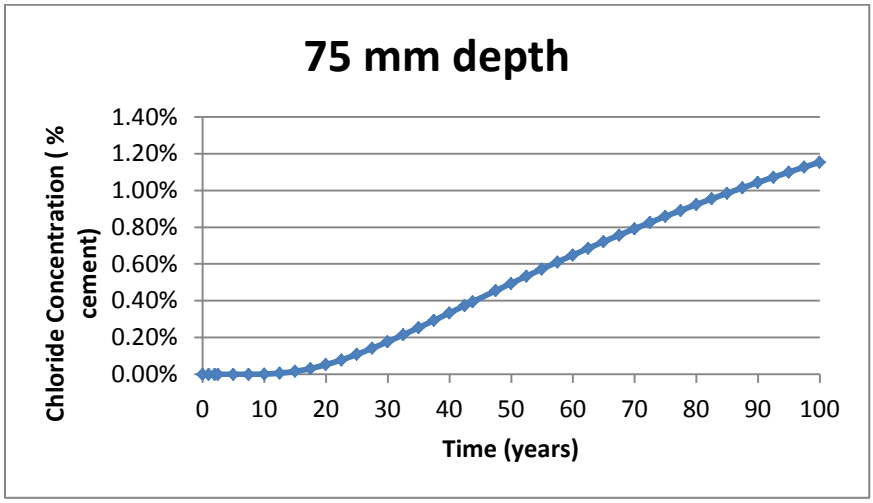
75 mm depth
Chloride Concentration (% cement)
1.40%
1.20%
1.00%
0.80%
0.60%
0.40%
0.20%
0.00%
0
10
20
30
40
50
60
70
80
90
100
Time (years)

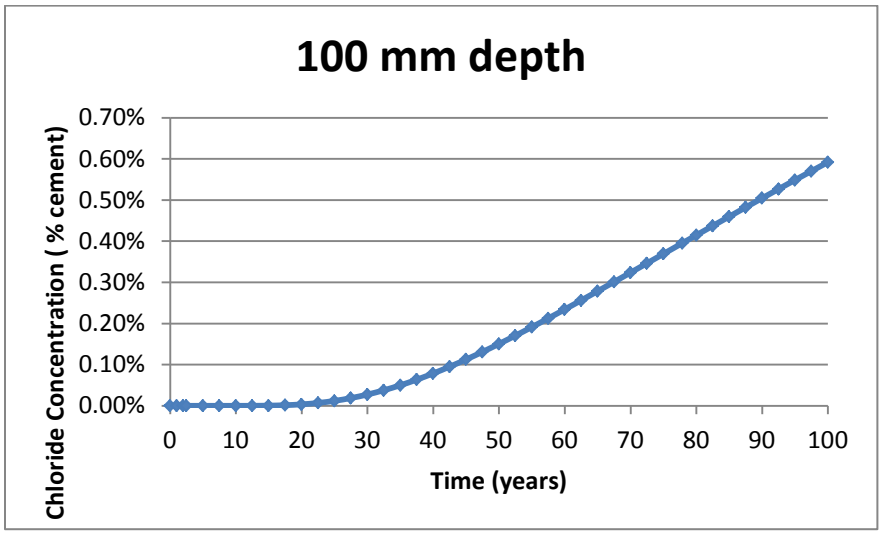
100 mm depth
Chloride Concentration (% cement)
0.70%
0.60%
0.50%
0.40%
0.30%
0.20%
0.10%
0.00%
0
10
20
30
40
50
60
70
80
90
100
Time (years)

The length of initiation stage (time to activate the corrosion) for various concrete cover depth is depicted in below, assuming the chloride threshold level for corrosion equates to 0.4% by weight of cement.

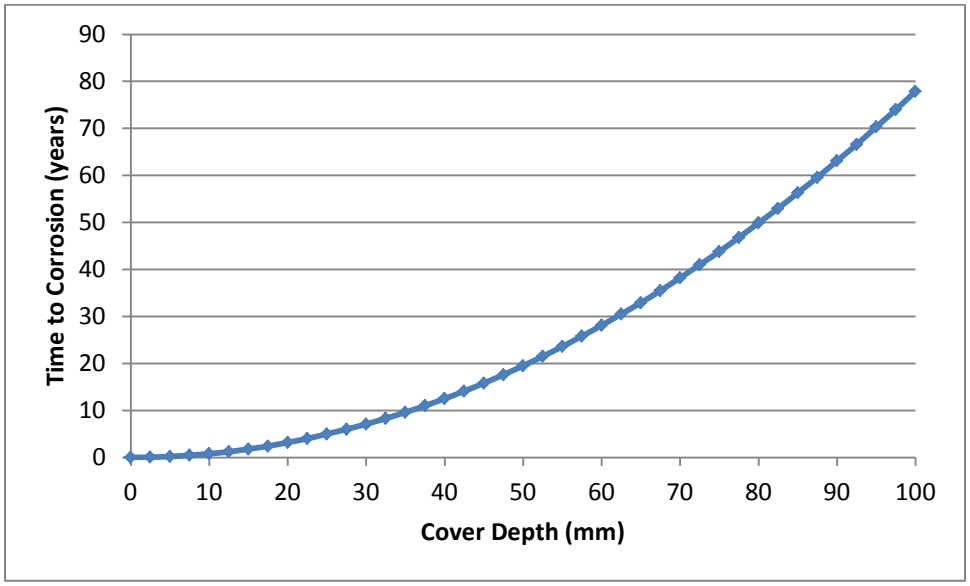

1.2 Corrosion Propagation Stage

Based on study conducted by Chen et al (2007), it can be referred that the diameter loss of rebar after corrosion is calculated as below:

$$D_{loss} = 5.9 \times 10^{-11} \cdot i_{corr} \cdot t \cdot R \qquad (5)$$

where i_{corr} is the corrosion rate and many researchers adopted it as a constant value as i_{corr} = 0.01 A/m^2. t is time in seconds and R is considered as a magnified ratio based on different environment.

2 CONCLUSION

The long-term performance of reinforced concrete structure in marine environment, especially the bridge columns, can be generally predicted by following procedures:

1). take concrete cover to be 38 mm as measured from Krk Bridge

2). the length of corrosion initiation stage can be estimated from the first part, and time period is about 11.3 years.

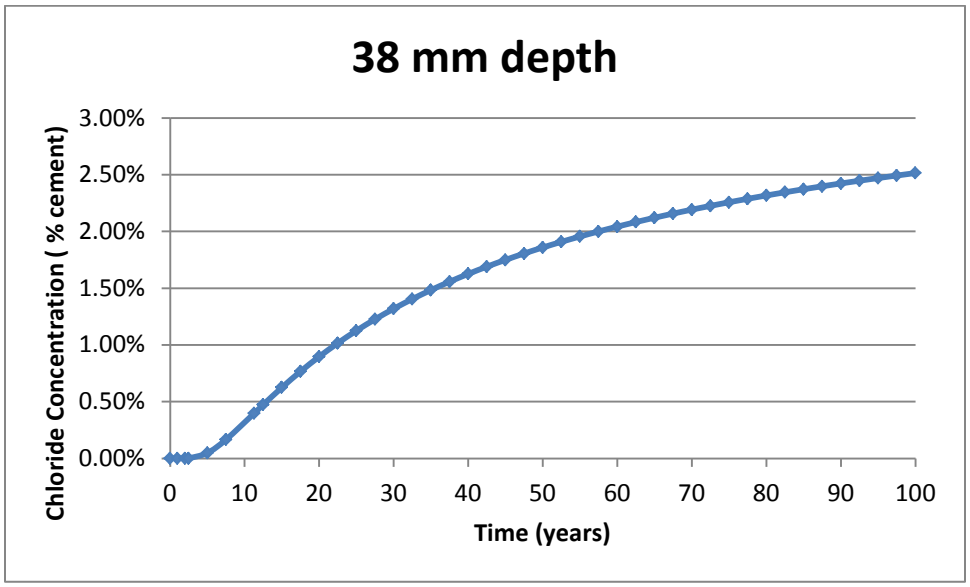

3). take original rebar diameter as 0.0508 m (#16) and plot the area remained ratio (reduced area/original area) per time, the magnified ratios are selected to be 1, 5, 10, 15, 20 respectively.

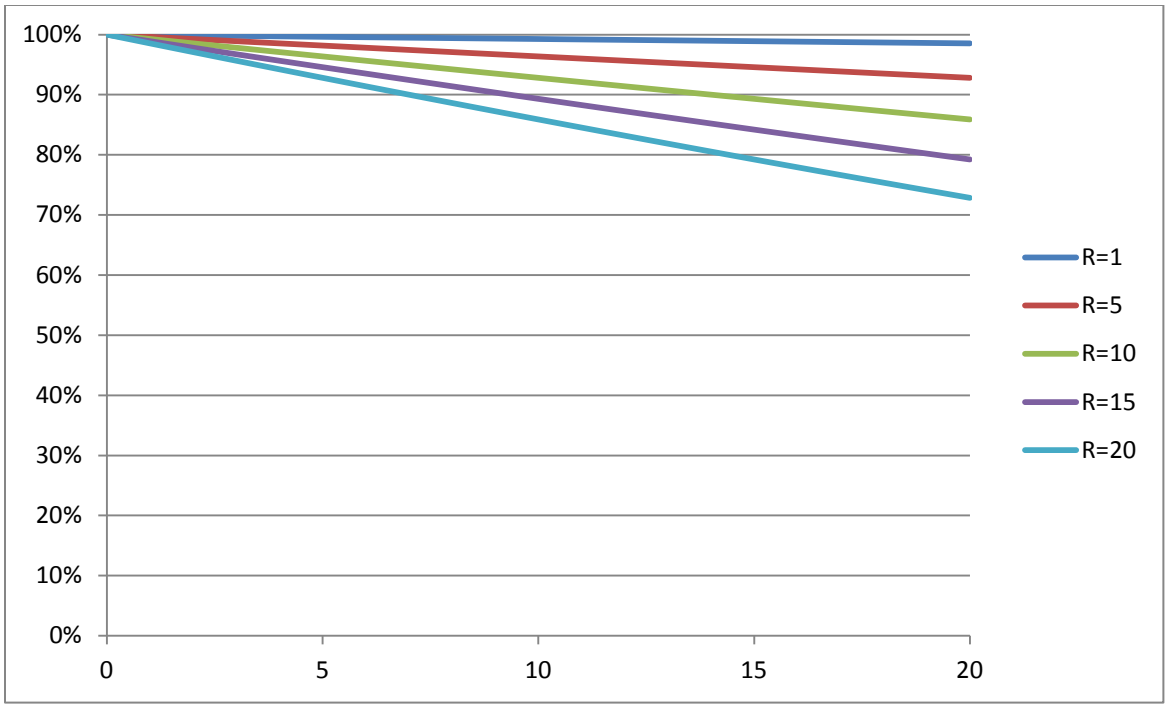

4). with the remaining rebar cross-section area known, one can calculate the compression strength of the bridge column as long as the cross-section layout is available.

BEHAVIOR OF CONCRETE FILLED FRP AND STEEL-CONCRETE-FRP CYLINDERS UNDER SEVERE ENVIRONMENTAL CYCLES

Concrete-filled fiber reinforced polymer tubes (CFFTs) have gain increasingly popularity in bridge construction during the past decade. The prefabricated fiber reinforced polymer (FRP) tubes have high strength-to-weight ratio, provide effective confinement to the concrete core, and have high resistance to environmental effects. CFFT bridge piles have been widely used as an alternative to conventional reinforced concrete columns recently in the United States, especially in the north-central part of the country, where bridge piles will experience freezing-thawing cycles during winter and high temperature during summer. Besides that harsh environment attack, wet-dry cycles will also be aggressive to bridge piles if the bridge locates in marine area or rivers.

The GFRP tubes in CFFT systems prevent ingress of moisture and ions into the concrete, which leading to an enhanced durability. However, the mechanical properties of glass fibers and polyester resin, the two constituents of the current commercial GFRP materials, can decrease when subjected to wet alkaline or saline environments.

The ester group, which is the weakest bond in polyester matrices, is prone to degradation by hydrolysis as shown in the following equation.

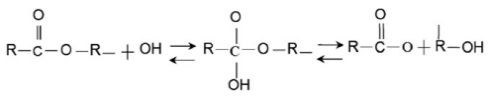

Eq. (1)

Epoxy is usually not affected by hydrolysis since there's no ester group in the molecular structure, but epoxy can absorb from 1 to 7% moisture by weight, which plasticizes the matrix, inducing differential swelling stresses, and generally degrading the physical properties (Soles et al. 1998).

Several researchers (Dejke 1999; Benmokrane et al. 2002) reported that the high alkalinity environment in the concrete core combined with outside saline solution produce lots of free hydroxyl ions (OH-), NaCl, and H2O molecules, which can diffuse through the polymer matrices and deteriorate glass fiber through leaching, etching and embrittlement mechanisms. The diffusion of the alkali ions out of the glass structure, known as ''leaching'', is the most important reaction in the dissolution of glass in water as shown in the following equation:

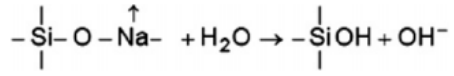

Eq. (2)

The second important reaction is called ''etching'', in which the hydroxyl ions break the Si–O–Si structure as shown in the following equation:

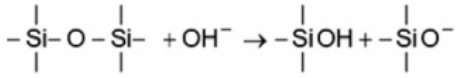

Eq. (3)

The embrittlement of fibers is attributable to the nucleation of calcium hydroxide on the fiber surface, which degrade the glass fibers in strength and toughness.

In addition, the deterioration at the interfaces between the fibers and the matrices involves a much more complex mechanism (Chen et al. 2007). The interface is a nonhomogeneous region with a thickness of approximately 1 μ m. This layer is weakly bonded and is most vulnerable to deterioration (Chen et al. 2007). The three dominant deterioration mechanism s included matrix osmotic cracking, inter-facial debonding, and delamination

(Bradshaw and Brinson 1997). The moisture diffusion into FRP composites could be influenced by anisotropic and heterogeneous character of the material. Along with diffusion into the matrix, wicking through the fiber/matrix interface in the fiber direction could be a predominant mechanism of moisture ingress (Apicella et al. 1982; Prian and Barkatt 1999). Nonvisible dissociation between fibers and matrix could lead to rapid losses of interfacial shear strength (Ash bee and Wyatt 1969).

In addition, there's only one research has been done on the effects of freezing and thawing cycles and sustained load on CFFT systems (Fam et al. 2008). In this investigation, the sustained load was incorporated by the way shown in the schematic figure below, and two different kind of concrete (normal weight, low strength and light weight, medium strength) were considered. The test results revealed that sustained axial load will improve compressive strength of the CFFT specimens due to creep effect, which tended to increase the radial strain of concrete and therefore induce active confinement imposed by the GFRP tube. Freezing and thawing effects will increase the compressive strength of cylinders even further, since the expansion of the freezing concrete core during thawing will add more pressure to the confinement pressure induced by the creep effect. However, in order to model the real weather situation, more weather conditions (i.e. wet and dry cycles, high temperature and ultraviolet radiation exposure) should also be considered besides freezing and thawing cycles in the above study.

Most recently, the hybrid FRP-concrete-steel double-skin tubular (DST) column was proposed by Teng et al. (2004) as a new type of composite system. This column system consists of inner steel tube, outer FRP tube and concrete in between, which combines the advantages of all the three component materials to achieve a superior mechanical performance. However, the

performance of this new type of structure member after aggressive environmental effects has not been studied yet.

The purpose of this paper is to investigate the combined effects of freezing-thawing cycles, high temperature, wet-dry cycles, and sustained axially load on both CFFT and DST columns. Two main tests were conducted: axial compression test on cylinders and hoop tensile test on ring specimen cut from out FRP tube, on both type of columns after conditioning. The same tests were also conducted on two groups of control specimen: one set with environmental conditions but without load, and another set keeping in room temperature without load. Other test including Microwave Non-Destructive Testing, Scanning Electron Microscopy (SEM), Differential Scanning Calorimetry (DSC), and Fourier Transform Infrared Spectroscopy (FTIR) have been done to detect the physical, thermal, and chemical properties changes on outer FRP tube material. The experimental work is first presented in this paper, followed by the test results and the discussion.

1 MATERIAL PROPERTIES

1.1 FRP tube

The outer FRP tubes for all of the CFFT and DST cylinders were Glass Fiber Reinforced Polymer (GFRP) tubes manufactured by Fiber Glass System. The tube was fabricated by filament winding process using isothalic polyester thermosetting resin to impregnate strands of continuous glass filaments. The winding angle was $\pm 45^{\circ}$ in which a certain amount of axial load capacity can be provided. The pipe wall included an internal resin-rich corrosion barrier. The detailed size information and mechanical properties are shown in Table 1. Coupon and ring specimens were cut from the tube in longitudinal and hoop direction, respectively. ASTM

D3039/D3039M-14 (ASTM 2014a) was followed to conduct coupon tensile test and hoop tensile test was done based on ASTM D2290-12 (ASTM 2012). Three specimens were performed for each test and the average values were taken.

Table 1. Dimension and Mechanical Properties of the FRP Tubes

Tube Application	d_o (in)	t (in)	f_L (ksi)	E_L (ksi)	e_L (%)	f_H (ksi)	E_H (ksi)	e_H (%)
CFFT	6 .625	0 .135	8 .43	1 523.33	0 .71	4 1.91	2 128.90	0 .97
DST	8 .5							

Note: d_o = outer diameter; t = wall thickness; f_L and f_H = ultimate tensile strength in longitudinal and hoop directions, respectively; E_L and E_H = elastic modulus in longitudinal and hoop directions, respectively; e_L and e_H = failure strain in longitudinal and hoop directions, respectively.

1.2 Steel Tube

The outer diameter of the steel tube is 4 in and the wall thickness is 0.15 in. Three 4 in × 16 in steel tubes were tested under monotonic compressive load at a 0.02in/min displacement rate. Two specimens were failed by local buckling in the elephant's foot mode at the ultimate compressive loads 67.80 kips and 66.50 kips, corresponding to 73.31 ksi and 71.91 ksi

compressive strength, respectively. The third sample was failed by global buckling and local buckling at elephant's foot mode, however, with a much lower ultimate load capacity 18.55 kips. Three coupon specimens were also cut from the tube in the longitudinal direction and tensile tests were conducted according to ASTM A370-14 (ASTM 2014b). Tensile properties of the steel coupon are shown in Table 2.

Table 2. Tensile properties of the steel coupon

Elastic Modulus (ksi)	Yield Strength (ksi)	Ultimate Strength (ksi)	Ultimate Strain (%)
29,000	90	90	0.40

1.3 Self-Consolidating Concrete (SCC)

Self-Consolidating Concrete (SCC) was used to cast all of the CFFT and DST cylinders. The mix design is shown in Table 3. All the cylinders were casted in three separated dates because of material and time availability. In order to have very similar concrete for all the times, slump flow diameter was controlled for each time to be 26 in by slightly adjusting the amount of HRWRA and VEA. In addition, six 4 in × 8 in small plain concrete cylinders were casted to test the compressive strength at 28th day and the day of test. ASTM C39/C39M-14a (ASTM 2014c) was followed to test the 28th day compressive strength of nine small cylinders (three from each

date), and the results showed very good agreement with average 6,646 psi, 6,870 psi and 6,723 psi, respectively.

Table 3. SCC mix proportions

w/cm	Cement (lb/cy)	Fly Ash (lb/cy)	Water (lb/cy)	Fine aggregate (lb/cy)	Coarse aggregate (lb/cy)	HRWRA (lb/cy)	VEA (lb/cy)
0.38	590	295	336	1411	1411	3.6	1.2

2 EXPERIMENTAL PROGRAM

2.1 Specimen Preparation

There were three different groups of cylinders in the whole experimental work: un-conditioned without load, conditioned without load, and conditioned with load. Each group had four specimens for both CFFT and DST types: three 12 in height for compression test and one 9 in height for hoop tensile strength test. In order to remove any unrelated moisture and temperature influence on GFRP tubes except environmental chamber, all the cylinders were

cured in room temperature and covered with plastic cloth only rather than keeping in the moisture room. In addition, for the purpose of simulating real-life CFFT or DST bridge piers in which concrete isn't exposed to outside environment, the top and bottom surface of the cylinders were coated with a thin layer of Sikagard 62 epoxy coating, as shown in Fig. 1b. Concrete grinding machine was used to grind both surfaces to be smooth and flat before coating (Fig. 1a).

(a) (b)

Fig. 1. Specimen preparation: (a) CFFT cylinders with grinded concrete surfaces; (b) epoxy coating on concrete surfaces

2.2 Instrumentation and Test Setup at Environmental Chamber

In order to apply load on cylinders while being conditioned, double steel plates with post-tensioned DYWIDAG bars were instrumented for four cylinders in series. Fig.2 illustrates the schematic and actual pictures of the setup. The load was applied by the hydraulic jack and monitored by a load cell. The axial load was designed to be 1 ksi, which is about 10% of

designed axial load capacity of the cylinder. This percentage is a typical value for real-life bridges where actual loading is around 10% of the design capacity. After the designed load was reached, the three nuts on top of the top triangle plate were tightened and the jack, load cell together with the anchor plate were removed. Three sets of washer springs were put between middle and bottom plates in order to sustain the load. Strain gauges were also instrumented on each DYWIDAG bar to monitor the load relaxation and the setup was loaded again if necessary. Neoprene rubber pads were put between cylinders and steel plates for better leveling and contact.

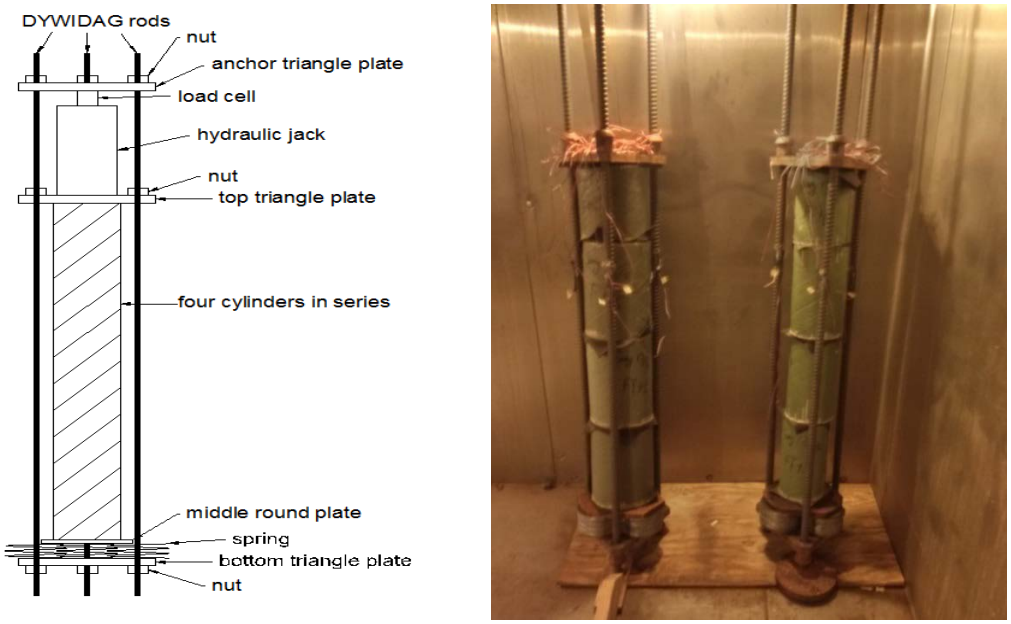

Fig. 2. Loading setup for environmental chamber

In addition, cylinders which were designed to undergo conditioning without load were also put into the environmental chamber. In order to obtain a more accurate compressive strength of concrete at the day of compression test, six 4 in × 8 in small plain concrete cylinders with same epoxy coating all around were kept in the environmental chamber as well (Fig. 3).

2.3 Weather Exposure Regime

The complete environmental conditioning regime consists of one set of freezing-thawing cycles, three sets of high temperature cycles and three sets of relative humidity (RH) cycles. There are 50 cycles for each set of condition. Figure 3 illustrates the complete conditioning regime and the temperature ranges for each set of cycles are shown in Table 4. The freezing-thawing, high temperature and high RH are aimed to simulate winter season, summer season and rain weather changes for 20 years. The total running time for the complete conditioning process was about 72 days.

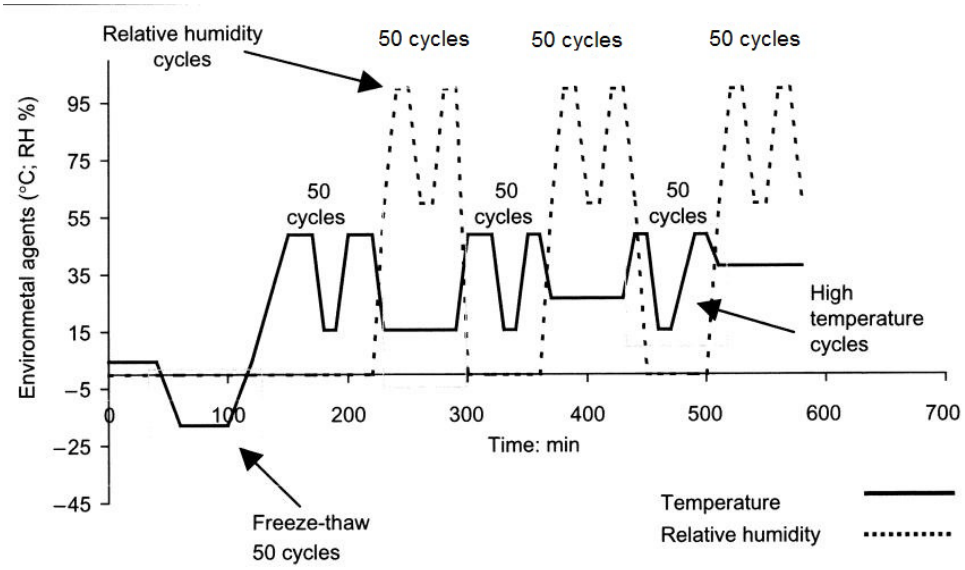

Fig. 3. Exposure regime for environmental chamber

Table 4. Temperature and RH range for each conditioning cycles

Condition Type	Freezing-Thawing	All Temp.	1st RH	2nd RH	3rd RH
Temperatur	-4 F to	68 F	60 RH	60 RH to	60 RH to

e/RH Range	50 F	to 122 F	to 95 RH @ 68 F	95 RH @ 77 F	95 RH @ 104 F

2.4 Instrumentation and Setup for Compression and Hoop Tensile Tests

After environmental conditioning, all of the cylinders were taken out from the chamber and conducted compression test on 12-in height cylinders and hoop tensile test on 9-in height cylinders. The concrete core of 9-in height cylinders was crushed by portable concrete drilling machine first to separate the concrete core and the GFRP tube, and then the GFRP tube was cut into 1-in width ring specimens in order to do the split tensile test.

As for compression test, two linear variable displacement transformers (LVDTs) were instrumented to the test setup to test the vertical displacement, two strain gauges were bonded to the mid-height of GFRP surface in hoop direction to test the hoop strain. In addition, two strain gauges were applied to the mid-height of inner steel tube in longitudinal direction for DST cylinders to monitor the strain change of the inner steel tube. A tiny hole was drilled through each DST cylinder so as to pull the strain gauge wires out. Fig. 4 shows the test setup.

(a) (b)

Fig. 4. (a) Setup for compression test on cylinders; (b) Tiny hole on the DST cylinder

For each group of cylinders, two of the three were applied monotonically increasing load at a 0.02 in/min displacement rate until failure, and the other one was undergone cyclic compressive loading with 0.02 in/min displacement rate and three cycles for each designed displacement level.

On the other hand, split tensile test on GFRP ring specimen was conducted in the way shown in Fig. 5. Two semicircle stainless steel plates were embedded inside the ring specimen and would pull the ring in tension while the loading head was moving apart. Strain gauges were

bonded to the ring specimen where two steel plates met. The load was increased monotonically with 0.1 in/min displacement rate until specimen failure.

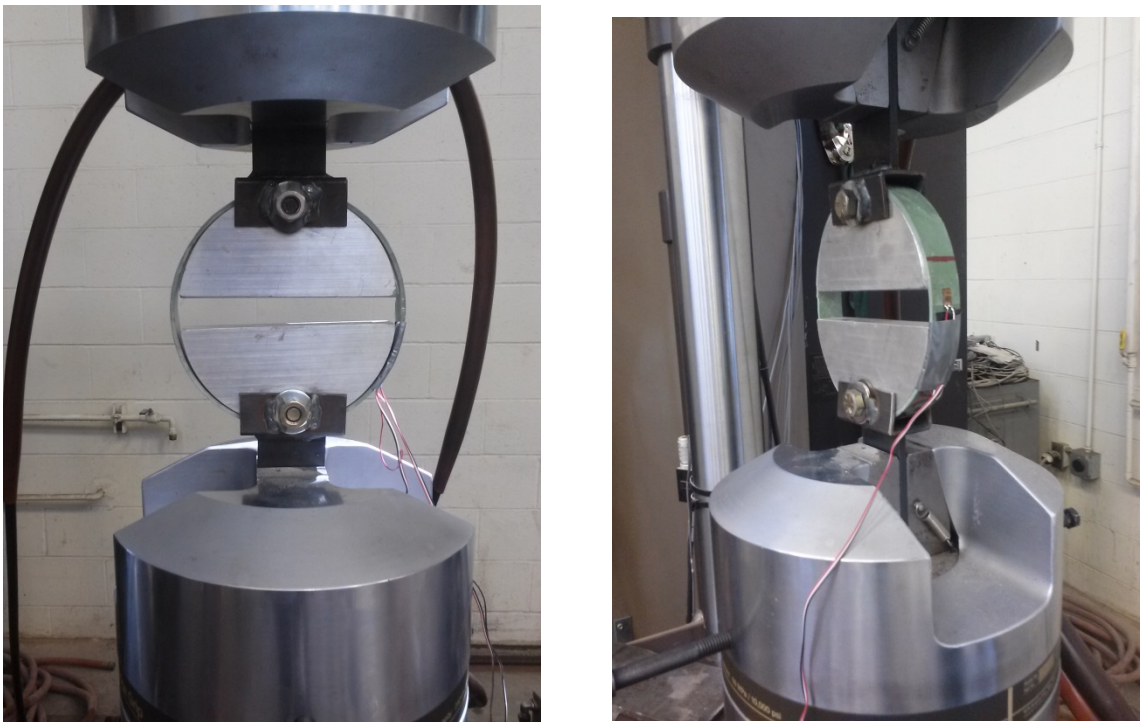

Fig. 5. Loading setup for hoop tensile strength test on GFRP rings

3 TEST RESULTS AND DISCUSSION FOR CFFT

3.1 Failure Modes

All the CFFT cylinders failed by GFRP tube rupture and followed immediately by diagonal shear fracture of the concrete core. This might attribute to high confining effect of the GFRP tube to the concrete core, and once the outer confinement disappeared, the core concrete cylinder broke suddenly due to very large load. Fig. 6 demonstrates GFRP tube rupture together with concrete core failure mode for each cylinder. Table 5 summarizes the maximum compressive strength, maximum vertical strain and associated strain and strength, respectively,

for cylinders under monotonic loading. In addition, stress-strain curves for each of those cylinders were depicted in Fig. 7 for comparison. The name of the cylinder was in type of "CFFT_XX_#" with "XX" standing for conditioning situation (FT+S = Freezing-Thawing plus Stress; FT = Freezing-Thawing only; UC = Unconditioned) and "#" standing for sample number.

(a)

(b)

(c)

(d)

(e)

(f)

(g)

Fig. 6. Failure modes of outer GFRP tube and core concete cylinder for CFFT specimens: (a) CFFT_UC_1; (b) CFFT_UC_2; (c) CFFT_FT_1; (d) CFFT_FT_2; (e) CFFT_FT_3; (f) CFFT_FT+S_1; (g) CFFT_FT+S_2

Table 5. Mechanical Properties in vertical direction for CFFT cylinders under monotonic load

Cylinder	Maximum Strength (ksi)	Strain at Maximum Strength	Strength at Maximum Strain (ksi)	Maximum Strain
CFFT_UC_1	11.58	0.74%	7.54	1.88%
CFFT_UC_2	12.11	0.74%	8.77	1.68%
CFFT_FT_1	9.64	0.54%	8.60	1.56%

CFFT_FT_2	10.27	1.08%	8.72	1.38%
CFFT_FT+S_1	10.54	0.64%	8.53	1.34%

Note: CFFT_FT+S_3 was crushed by the loading machine accidently and no results obtained.

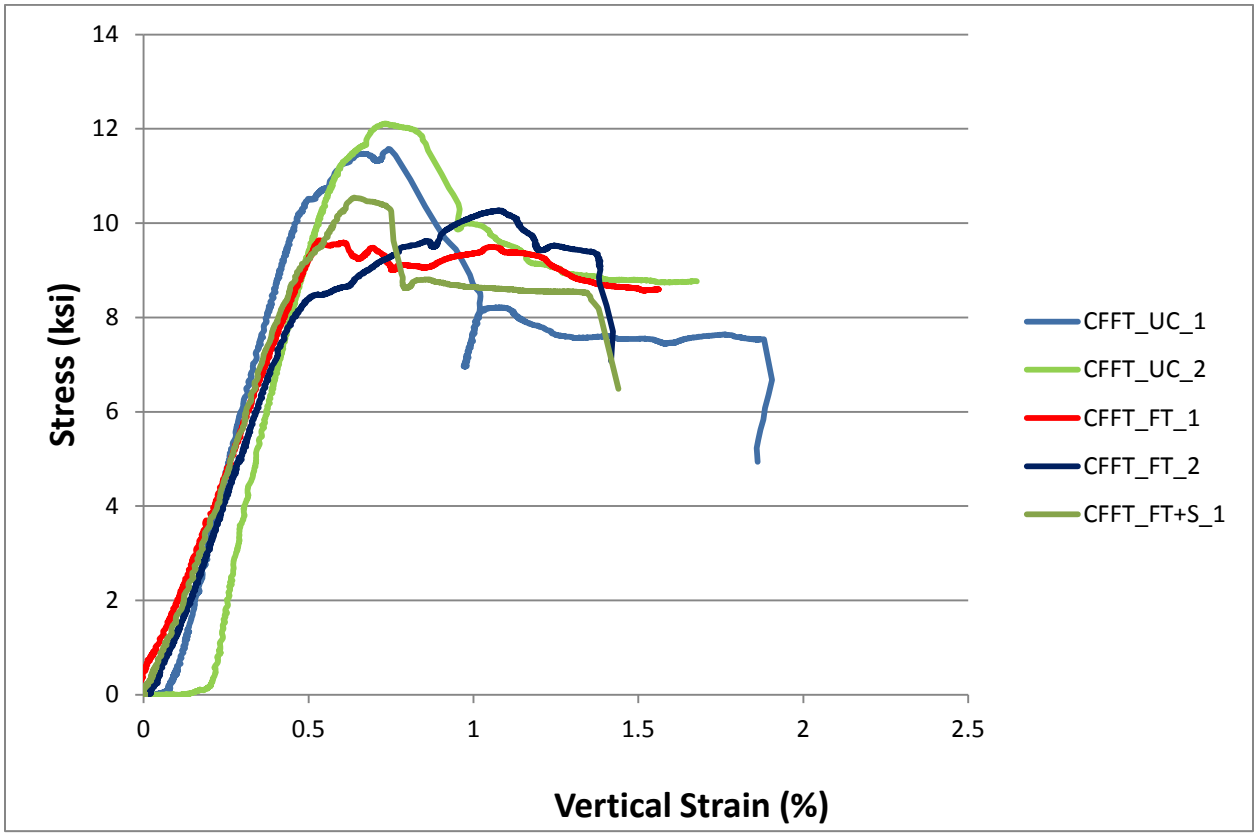

Fig. 7. Stress-strain behavior in vertical direction for CFFT cylinders under monotonic load

It can be noticed from Table 5 and Fig. 7 that, all CFFT cylinders underwent environmental conditioning had certain amount of degradation in both maximum strength and

maximum strain. The maximum strength and strain degradation for cylinders with conditioning and stress are 11% and 25%, respectively, compared with the average value for unconditioned ones, and the degradation percentage for cylinders with conditioning only are 16% for maximum strength and 17% for maximum strain. These show that the outer GFRP tube did have degradation in both strength and strain after environmental conditioning. Although the differences between conditioned cylinders with stress and without stress are not that considerable, this might due to the lack of representative samples so that the loading effect is not noticeable.

3.2 GFRP Tube Rupture in Hoop Direction

The strain history of the outer GFRP tube in hoop direction was also recorded by strain gauges and the average values are plotted versus compressive strength as shown in Fig. 8 below.

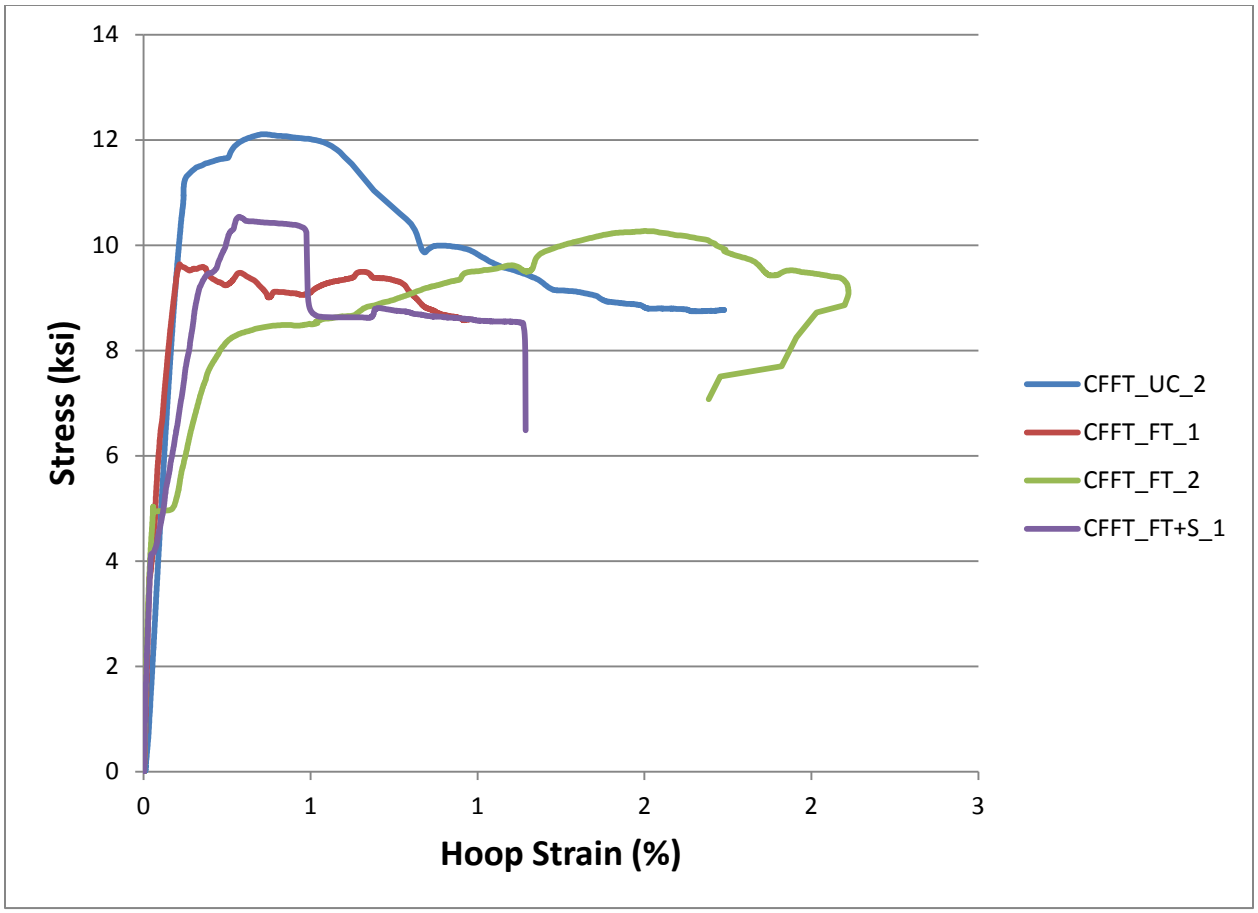

Fig. 8. Stress-strain behavior in hoop direction for CFFT cylinders under monotonic loading (Note: the strain data for CFFT_UC_1 was lost due to out of order of the strain box)

It can be seen from Fig. 8 that the elastic modulus in hoop direction for all the GFRP tubes were basically the same, which further verified there's no degradation in elastic modulus for all the CFFT cylinders in vertical direction as shown in Fig. 7. One can also noticed that the CFFT cylinders experienced environmental conditioning only had decreased ultimate hoop strain, which was 11% compared with unconditioned ones, while the value for cylinders with combined conditioning and stress was 33%. This explains the reduced maximum strain in vertical direction for conditioned CFFT specimens.

3.3 Energy Dissipation Capacity

As mentioned before, one of the three cylinders for each condition situation was loaded with cyclic loading in order to investigate the energy dissipation capacity. The dissipated energy curves for each deformation level were depicted for both combined conditioning with stress and conditioning only (Fig. 9). The dissipated energy was calculated as the area circled by each loop cycle and the average value was taken from every three cycles. The cyclic compression loading was not able to be performed on the unconditioned cylinder when this paper was writing. However, it still can be seen from the figure below that the CFFT cylinders with conditioning only can sustain more cycles of loading and dissipated more energy at higher level of deformation than CFFT cylinders with combined conditioning and stress, which might attribute to the sustained load intensified the degradation of the GFRP tube by causing more cracks on the surface and absorbing more moisture and aggressive ions.

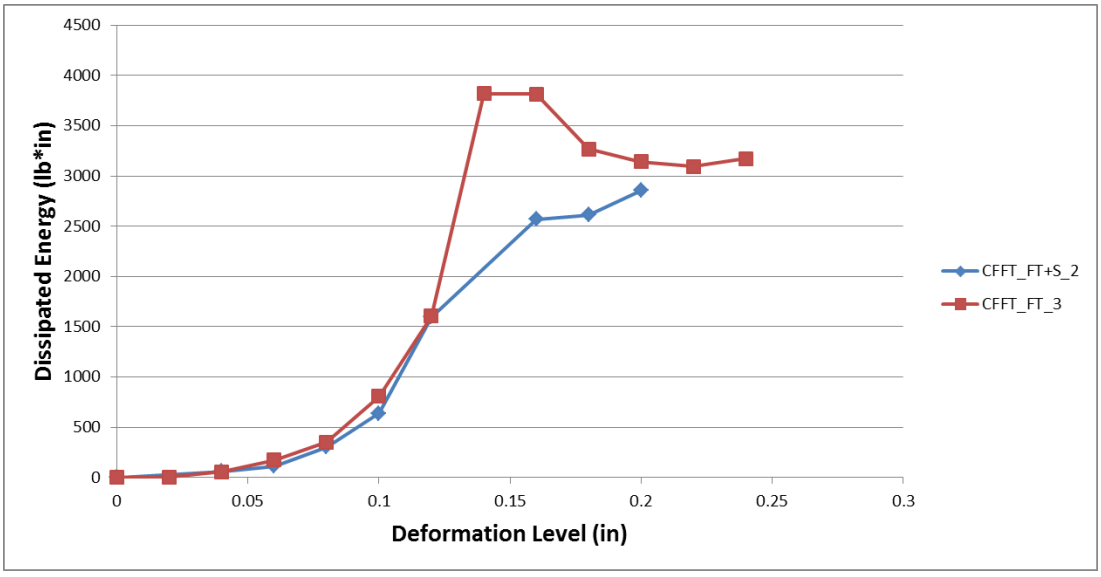

Fig. 9. Dissipated energy at each deformation level for CFFT_FT+S_2 and CFFT_FT_3

3.4 Tensile Properties in Hoop Direction for Ring Specimens

Hoop tensile test on ring specimens cut from CFFT cylinders is another effective way to study the mechanical properties change in GFRP material. Three ring samples were cut from 9 in height CFFT specimens of both conditioning only and unconditioned cases. The ring samples were not able to cut from CFFT cylinders of combined conditioning and stress at the time of writing this paper. The mechanical properties, including maximum strength, maximum strain and elastic modulus, are shown in Table 6 below.

Table 6. Mechanical Properties in Hoop Direction for GFRP Tubes

Specimen	maximum stress (ksi)	max strain	Elastic Modulus (ksi)
CFFT_UC_1	45.75	0.82%	2240.96
CFFT_UC_2	50.88	1.75%	2442.83
CFFT_UC_3	35.09	0.87%	1562.63
AVERAGE	43.91	1.15%	2082.14

CFFT_FT_1	40.30	0.7 1%	1943.10
CFFT_FT_2	35.86	1.2 7%	2214.36
CFFT_FT_3	32.28	-	-
AVERAGE	36.15	0.9 9%	2078.73

Note: the strain gauge for CFFT_FT_3 did give good reading and was discarded from this table

It can be proved from this table again that the elastic modulus of the GFRP tubes didn't reduce after conditioning. The maximum hoop tensile stress of conditioned samples reduced about 18% and maximum strain reduced about 14% compared with unconditioned samples.

4 TEST RESULTS AND DISCUSSION FOR DST

4.1 Failure Modes

Similar to CFFT cylinders, outer GFRP tube rupture was the failure mode for all the DST cylinders, and there was no damage or buckling occurred on the inner steel tubes. However, the

concrete between two tubes were crushed into multiple columns before the GFRP tube ruptured. This might due to several reasons: 1) the shape and size of the concrete block was very slim and easy to be broken; 2) there was not enough horizontal pressure from inner steel and hollow core; 3) the hydrostone capping on top of the DST cylinder may transfer larger amount of the load to the concrete block than outer GFRP tubes and inner steel tubes, due to the very tiny contact area and sharp edges. The observed damage situations for all the DST cylinders were shown in Fig. 10. In addition, the mechanical properties and stress-strain behavior of DST cylinders under monotonic loading are shown in Table 7 and Fig. 11.

(a)

(b)

(c)


Song 12/15
FT2
Song 12/15
FT2

(d)


FT3
FT3

(e)


Song 12/04
FTx51
Song 12/04
FTx51

(f)


Song 12/04
2
FTx5
Song 12/04
2
FTx5

(g)


3
3

(h)

Fig. 10. Failure modes for GFRP tubes and concrete block for all DST cylinders: (a) DST_UC_1; (b) DST_UC_2; (c) DST_FT_1; (d) DST_FT_2; (e) DST_FT_3; (f) DST_FT+S_1; (g) DST_FT+S_2; (h) DST_FT+S_3

Table 7. Mechanical Properties in vertical direction for DST cylinders under monotonic load

Cylinder	Maximum Strength (ksi)	Strain at Maximum Strength	Strength at Maximum Strain (ksi)	Maximum Strain
DST_UC_1	8.71	0.59%	6.27	1.40%
DST_FT_1	9.51	0.90%	8.71	1.11%
DST_FT_2	9.58	0.77%	8.07	1.04%
DST_FT+S_1	7.53	1.03%	7.28	1.68%
DST_	9.13	0.87%	6.33	2.

FT+S_2	00%

Note: DST_UC_2 sample was not able to be performed for compressive test at the time of writing this paper

From the Table 7 and Fig. 11, one cannot see noticeable degradation in compressive strength for DST cylinders after conditioning. Instead, the specimens experienced conditioning only even demonstrated 10% increase compared with unconditioned cylinders. DST_FT specimens had an 23% deduction in maximum strain from unconditioned cylinders and DST_FT+S had an 31% increase in maximum strain compared with unconditioned ones. Unlike the CFFT cylinders in which failure mode was mainly controlled by the rupture of outer FRP tube, the DST cylinders have difference failure mode and failure sequence for concrete block, and the embedded inner steel tube may make more effective contributions to the compressive capacity in structural level when the outer FRP tube was deteriorated. These make the mechanical properties of the DST specimen complicated and sometimes hard to explain the observed situations.

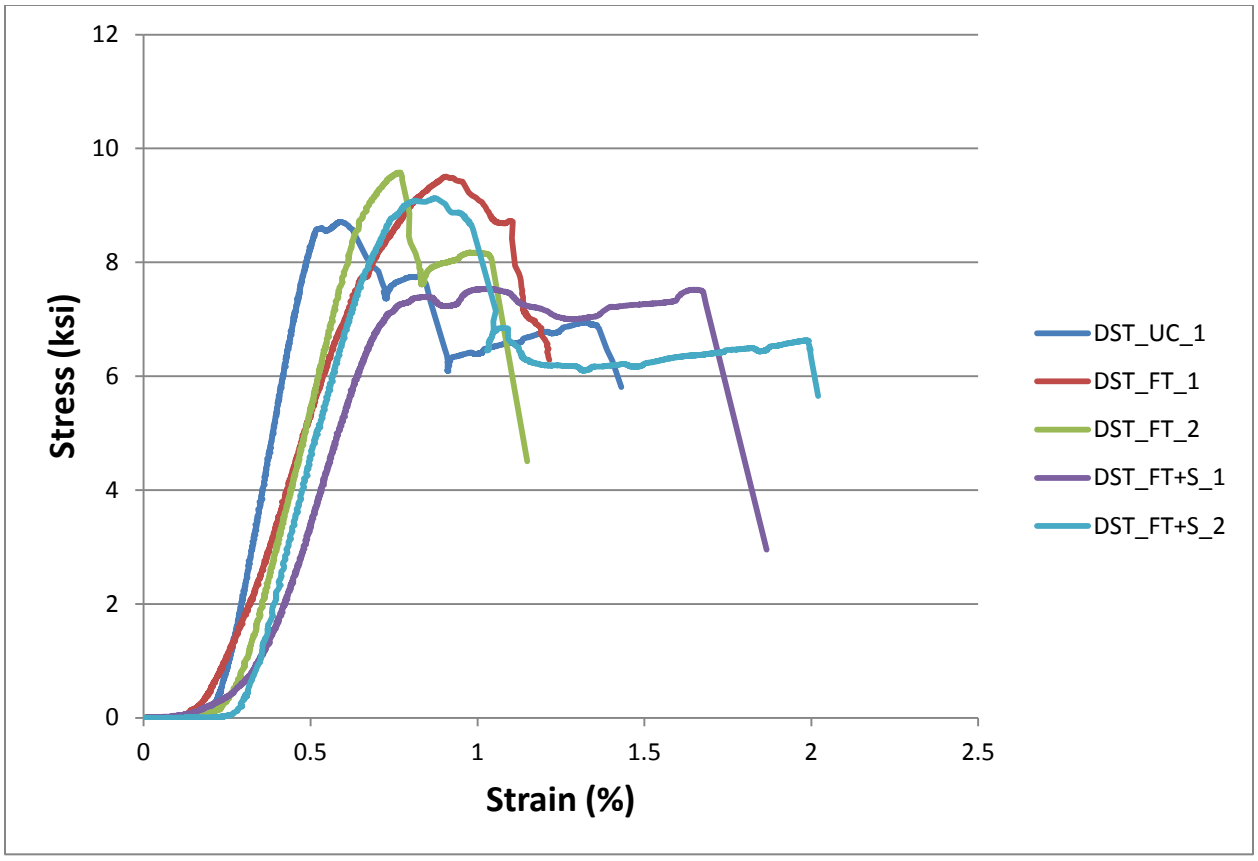

Fig. 11. Stress-strain behavior of DST cylinders under monotonic loading

4.2 GFRP Tube Rupture Strain in Hoop Direction

The strain readings in hoop direction for each DST cylinders were recorded and plotted in Fig. 12. It can be observed that the maximum hoop strain for DST_FT specimens decreased by 27% from the unconditioned samples, and the DST_FT+S samples increased by 25%. This trend is similar to the observation in vertical direction, which is still hard to explain.

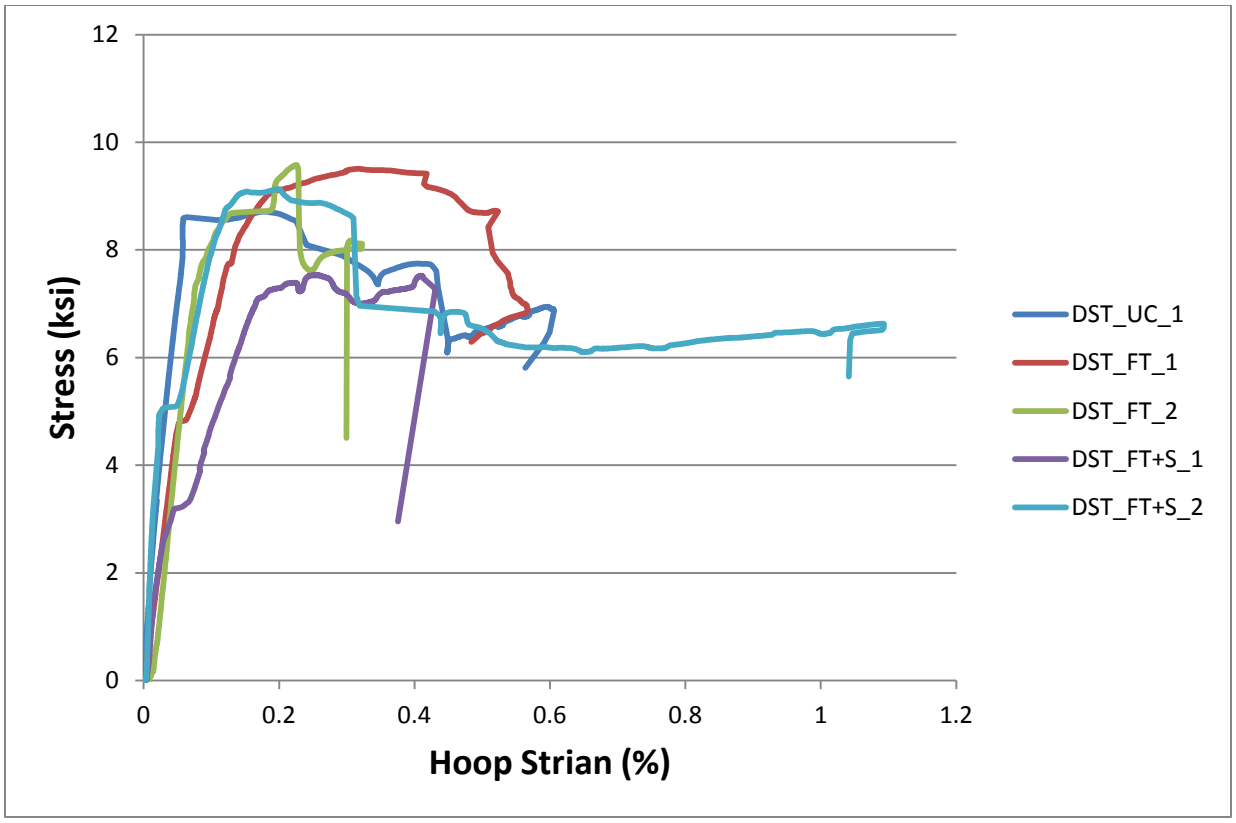

Fig. 12. Stress-strain behavior of GFRP tube in hoop direction for DST cylinders under monotonic loading

4.3 Stress-Strain Behavior of Inner Steel Tube

The test results showed that there was no damage or buckling situation happened on the inner steel tube for all of the DST specimens. Fig. 13 illustrates the stress-strain behavior of outer GFRP tube and inner steel tube in longitudinal direction for all the DST cylinders. From the figure, it can be seen that all the steel tubes deformed much smaller than outer GFRP tubes. Be noticed that the strain history in inner steel tube was obtained from mid-height strain gauges while the deformation for the GFRP tube is a global value, which is obtained from vertical LVDTs. This small strain change for inner steel tube might due to the friction or bond strength between steel tube and concrete, where the force grows larger and larger from top of the steel

tube to bottom of the steel tube, which can resist part of the compressive load and makes the strain distribution uneven through the tube height, with largest strain change at the top and minimum at the bottom.

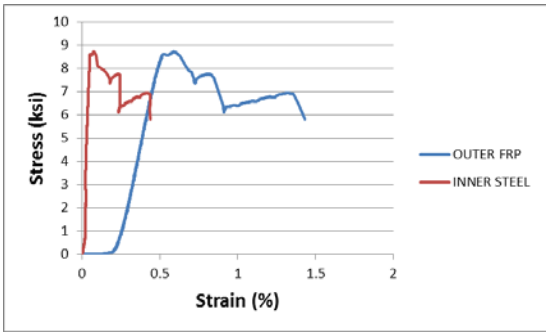

(a)

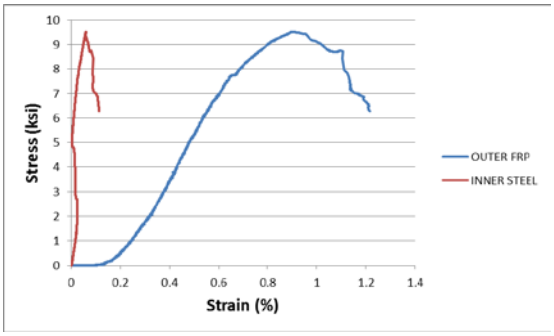

(b)

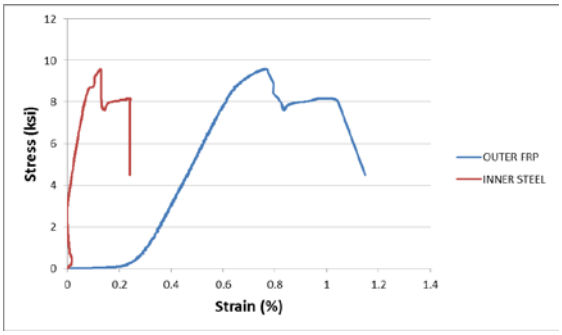

(c)

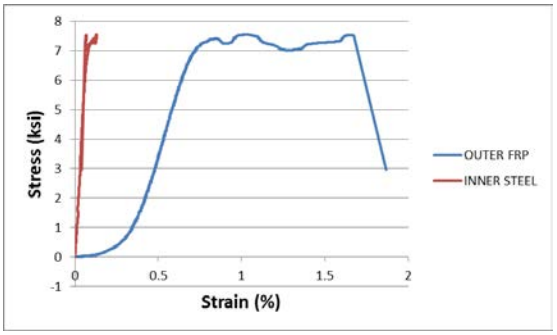

(d)

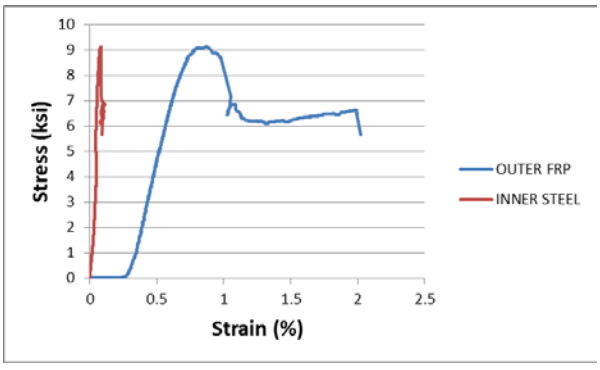

(e)

Fig. 13. Stress-strain behavior for outer FRP tube and inner steel tube in vertical direction for DST specimens under monotonic loading: (a) DST_UC_1; (b) DST_FT_1; (c) DST_FT_2; (d) DST_FT+S_1; (e) DST_FT+S_2

4.4 Energy Dissipation Capacity

The dissipated energy at each deformation level for all conditioning type cylinders under cyclic loading are plotted in Fig. 14. It can be observed from the curves that both conditioned only and combined conditioning and stress exhibited larger amount of dissipated energy than un-conditioned cylinder at larger deformation level. In addition, DST_FT specimen shows more power in dissipating energy than DST_FT+S specimen, which matches with the CFFT situation.

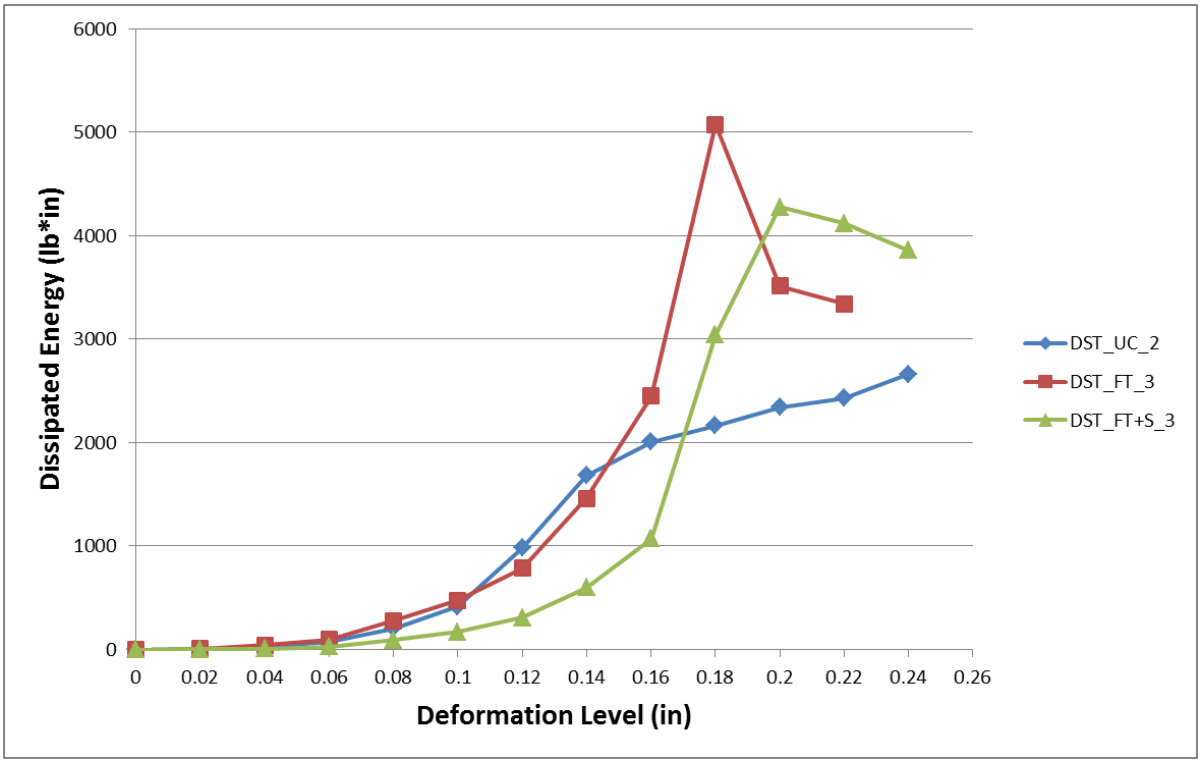

Fig. 14. Energy dissipation capacity at each deformation level for DST cylinders under cyclic loading

Conclusion

Experimental work has been done to investigate the combined freezing-thawing cycles, high temperature cycles, and high RH cycles on the mechanical properties of both CFFT cylinders and DST cylinders. Several conclusions can be drawn and shown as below:

1. Combined weather conditioning degraded the CFFT cylinders with GFRP tubes in both maximum strength and maximum strain, with around 10% – 20 % degradation percentage.

2. Sustained load may not have substantial effect on static mechanical properties of CFFT and DST cylinders, but do affect the dynamics properties, where the cylinders without sustained loading history showed more powerful energy dissipation capacity.

3. The failure mode and behavior of DST cylinders are complicated and hard to understand the degradation mechanism.

BEHAVIOR OF CONCRETE FILLED FRP AND STEEL-CONCRETE-FRP CYLINDERS UNDER SEVERE ENVIRONMENTAL CYCLES

5 BACKGROUND

Life-cycle cost analysis (LCCA) is a technique that have been used by the bridge owners, maintenance and rehabilitation engineers, and designers to study the economically efficient alternative set of actions and their timing during the bridge's life to achieve the intended service life (Hawk, 2003). LCCA includes the set of economic principles and computational technique to find the economically efficient strategies and investment options to ensure the serviceability of the bridges or bridge components. However choice of the principle and computational technique depends on the availability of information, specific interest or requirements (in bridge network level, in bridge system level, or in bridge component level) of bridge owners and maintenance engineers.

To maintain the serviceability and safety requirements throughout its service life, a bridge or its components requires inspection, maintenance, repair, rehabilitation, and replacement which incurs series of expenditure during their lifecycles. NCHRP report 483 represents such events as the life-cycle activity profile as shown in Figure 1.

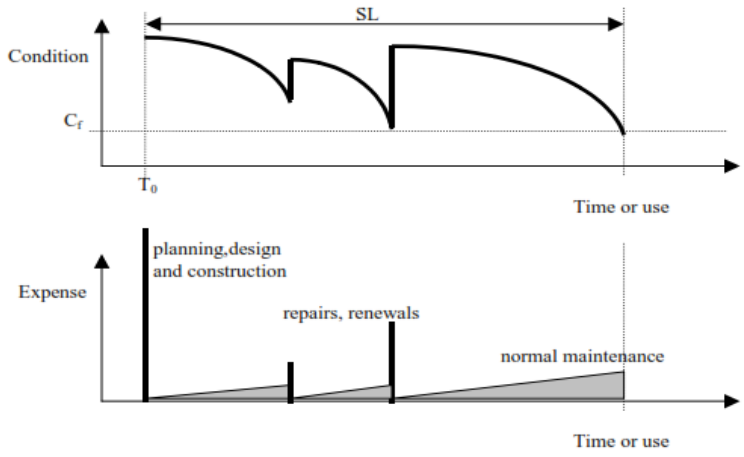

Figure 1. Life-cycle activity profile (Hawk, 2003)

Maintenance, repair and rehabilitation (MR&R) works on the bridges have been carried out to improve and maintain the acceptable condition or performance level throughout the intended service life. Measure of performance or condition may vary with the interest of bridge owners and their evaluation practices. However, in United States, mostly practiced performance measure is NBI condition ratings, scaled in 0-9, where 0 being "failed condition" to 9 being "excellent condition". Moreover, researchers and bridge engineer found to use safety index and reliability index as a measure of performance (Frangopol et al., 1997; Stewart, 2001; Liu & Frangopol, 2004). Evaluation of performance level, modeling of performance deterioration and minimum acceptable level of performance throughout the intended service life are necessary for the life-cycle analysis. The repair and rehabilitation works carried out on the bridges affect the performance curve: 1) instant improvement of the performance parameter or bridge condition, 2) delay in the performance deterioration, 3) reduction in the deterioration rate, and 4) loss of functionality of maintenance after a period of effective time i.e. life of repair. Optimization of such effects in terms of time of intervention, quality of intervention, and cost of intervention for alternative repair strategies is necessary for decision making process.

Decision making process requires the selection of best economic evaluation criteria to represent all the incurred life-cycle cost. Net present value (NPV), equivalent uniform annual cost (EUAC), internal rate of return (IRR), and benefit-cost –ratio (BCR) are the major evaluation criteria used in LCCA. Discount rate is used to account time value of money, and risks on the investment. Discount rate is the exponential value used to calculate present value of the future costs.

5.1 Scope

This study will be focused on the formulation of LCCA model to select the best repair strategy for chloride ion induced corrosion repair of RC bridge pier column. Chloride ion is present in marine water or snow and ice melt water where sodium chloride and calcium chloride have been used as deicing salts. Concrete cover loss due to cracking, spalling and delamination as a result of corrosion of reinforcement in RC elements is major deterioration phenomenon that affects the durability and load carrying capacity of the structural elements. Corrosion of reinforcement itself leads to loss in cross-section area and loss in mechanical properties of reinforcing steel and hence the structural elements becomes structurally as well as functionally deficient if no repair maintenance is considered. The Fiber Reinforced Polymer (FRP) composite is considered as the repair material. FRP composites are composed either of carbon fibers, glass fibers, or aramid fibers that are embedded in a resin matrix which binds the fibers together.

6 LITERATURE REVIEW

6.1 LCCA Methods

LCCA is a widely used tool in engineering for decision making while selecting competing alternatives. The LCCA and optimization method varies depending on the selection of performance parameter, and evaluation criteria for alternatives, however, in all case the LCCA includes all incurred cost and benefits throughout the life of structures. In the following paragraphs, reviews on different LCCA study, optimization and probabilistic simulation model will be discussed which considered condition rating, safety and reliability as a performance measure.

Mohammadi et al. (1995) developed a VI model in which three major variables: condition rating, bridge age, and cost were incorporated in terms of single parameter Value Index (VI). The VI was used to quantify the bridge decision-making process to come up with optimized strategy in managing repair and rehabilitation needs of a given bridge or bridge component. The objective function F which describe VI in terms of rating (r), time (t), and cost (c) is expressed as

$VI = F(r, c, t)$ and the form proposed for F is

$VI = r.t/c = A_s/c$

where, A_s = area under r.t (i.e. bridge/ bridge element deterioration curve)

The improvement in rating and life expectancy of the bridge was expected to increase the VI and expenditure on the bridge was expected to result in an improvement in its rating. The authors in this model suggested the iteration approach to optimize the objective function with

constraint of cost, time and target rating for different maintenance, repair and replacement (MR&R) events.

The authors also developed a computer program to perform bridge life-cycle cost analysis based on the VI model to investigate the planning decision for the deck repair work of one bridge from County Highway 1 over Interstate 55 at Sherman, Illinois. The latest allowable time for bridge rehabilitation was considered based on minimum rating required from the range of 1 to 9 (1 representing the worst condition) to fulfill the minimum serviceability and strength requirements. For the deterioration model as represented by $R(t) = 9- bt$, the authors defined the latest allowable time as given by the relation $T_{nmax} = n (9-R_{min})/b$ where, R_{min} was the critical condition rating. Selection of bridge life, deterioration curves for bridge elements, average daily traffic (ADT), MR&R cost data were the major inputs for the program. To calculate the cost of MR&R cost, authors used a simplified approach to determine the cost function for each MR&R cost $C_i(t_i)$ at time = t_i as,

$$C_i(t_i) = C_0\left(\frac{1+IR}{1+FR}\right)^{t_i} \frac{K(t_i - t_{i-1})}{9}$$

Where, C_0 = original cost; IR = interest rate; FR = inflation rate

Frangopol et al. (1997) studied the optimization methodology for the planning of inspection and repair works of deteriorating structures based on minimizing expected total life-cycle cost ensuring allowable lifetime reliability for the structures in acceptable limit. The authors estimated the expected total life-cycle cost (CET) as a sum of initial cost of structure (CT), the expected cost of routine maintenance (CPM), the expected cost of inspection (CINS), the cost of repair (CREP) and the expected cost of failure (CF). Optimization of the strategy considered is to minimize CET subject to $\beta life \geq \beta^* life$ where $\beta life$ and $\beta^* life$ are the lifetime

reliability index and the lifetime target reliability index respectively. The authors used this method to study the uniform and non-uniform inspection strategy for a prefabricated reinforced concrete T-girder bridge

The authors developed the event tree model to find out expected life- cycle cost to represent all possible events associated with repair and no repair actions followed by inspection. After each inspection, repair decisions were to be made whether or not the repair works of the structure required, and the decisions were considered to be influenced by the past events' decisions, whether or not the structure was repaired previously. If there are 'm' inspections in the life of structure, 2m represents the branches in the event tree. Each branch of the tree represents a specific sequence of events. The possibility of failure was expected before and after each inspection and repair event, and the probabilities of failure were calculated accordingly in each branch. The lifetime probability of failure was thus defined as the sum of failure probabilities of each branch of the event tree. The expected failure cost was calculated to be the product of failure probability and the cost of failure.

According to Stewart (2001), prioritization of inspection strategy, selection of optimal maintenance, repair or replacement can be carried out based on risk ranking and life-cycle cost tool using a risk based approach. In this study, reliability was used as a measure of bridge performance and hence used to prioritize risk management measures for maintenance, repair or replacement.

The author defined reliability in terms of probability of failure. Failure of a structural element considered to occur when the load effect exceeds the resistance. The author considered two different limit states for reliability analysis: ultimate limit states – flexural failure, shear

failure, and collapse, and serviceability limit states – cracking, durability, deflection, and vibration.

In the study, Stewart (2001) estimated the life-cycle cost (LCC) as a sum of cost of design (CI), cost of quality assurance (CQA), expected cost of inspection (CIN), expected cost of maintenance (CM), expected cost of repair (CR), and cost of failure (Cf) representing the probability of failure (pfLS) for each limit states (M) to occur up to any time tN. A constant discount rate (r) was considered for estimating the present value of the cost. The following expression was given by the author, which gives the life-cycle cost of any bridge 'k'.

$$LCC_k(t_N) = C_I + C_{QA} + \sum_{i=1}^{t_N} \frac{C_{IN}(t_i) + C_M(t_i) + C_R(t_i) + \sum_{LS=1}^{M} pf_{LS}(t_i) Cf_{LS}}{(1 + r^{t_i})}$$

The effectiveness of cover and w/c ratio in the concrete cracking was studied using life-cycle cost analysis. In the analysis, the Monte-Carlo simulation was used to obtain the probabilities of cracking for a RC bridge subjected to repeated application of de-icing salts.

Val & Stewart (2003) considered the time-variant probabilistic model to predict the expected cost of repair and replacement as an element of LCC. The proposed model was then used to optimize the strategies to improve the durability of RC structures in marine environments having carbon steel and stainless steel as reinforcement. The time-dependent probabilities of spalling of concrete were calculated up to 100 years of service life every year.

The authors proposed the expected cost of spalling as,

$$E_{SF}(T) = \sum_{i=1}^{T/\Delta t} \Delta p_{f,i} \frac{C_{SF}}{(1 + r)^{i\Delta t}}$$

where Δpf,i, is the probability of a spalling incident between the (i-1)th and ith inspections. Monte-Carlo simulation was considered to calculate the probability.

Mullard & Stewart (2012) presented the probabilistic reliability analysis to compare the effect of maintenance and repair strategies on timing, extent and cost over the service life. This spatial time-dependent reliability model found to considered concrete properties, concrete cover and surface chloride concentration as random fields while calculating the probability that a given extent of damage will occur for any time period. Monte-Carlo event based simulation was considered in the study. The authors presented the statistical variability of predicted LCCs for a RC bridge deck subject to a marine environment.

In spatial time-dependent reliability model suggested by Mullard & Stewart (2012), the corrosion initiation and propagation, crack initiation and propagation and influence of maintenance strategies were integrated into Monte-Carlo simulation. If the concrete surface is discretized onto k elements of equal size, then the proportion of a concrete surface with excessive cover cracking at time t is,

$$d_{crack}(t) = \frac{n\lfloor t > T_{i(j)} + T_{sp(j)} \rfloor}{k} \times 100\%$$

Where, Ti(j) and Tsp(j) = time to corrosion initiation and time to excessive cracking of element j, respectively and n[] = number of elements for which t > Ti(j) + Tsp(j) (timing of corrosion damage).

At the time of first repair, probability of damage incident between the (i-1)th and ith inspections

Δpf,I = Pr(dcrack(t) ≥ Xrepair\dcrack (t-Δt) < Xrepair)

where Xrepair is the percentage of a structure that is subjected to severe cracking before repair called repair threshold. The probability of damage hence incorporated in the LCC as suggested by Val & Stewart (2003). The authors also found to incorporate effect of maintenance in terms of repair efficiency factor ΔTi and γicorr , repair efficiency factor for corrosion initiation and repair efficiency factor for corrosion rate. After the repair, the Ti and icorr were found to be updated as,

$T_{i(repair)} = T_i + \Delta_{Ti} \qquad T_{i(repair)} > 0$

$i_{corr(repair)} = i_{corr} \times (100 + \gamma_{icorr})/100$

Engelund et al. (1999) found to use the probabilistic model to determine the optimal plans for repair and maintenance of bridge pier subject to chloride laden environment. The authors suggested that the optimal decision can be obtained by solving the optimization problem,

Min C

s.t $p_f \leq p_f^{max}$

where, C is the expected cost of repair and maintenance and pf max is the upper limit for some critical events.

$$C = \sum_{i=T_d}^{T_L} P(\,repair\ in\ year\ i\,)C_i$$

Where Td denotes the time in years where a decision about the repair strategy is made, TL denotes the design lifetime of the structures in years, and Ci denotes the cost of repair if it is performed in year i.

The authors found to use three different strategies for the maintenance of pier and service life of 50 years. The strategies were implemented if the criteria of damage were satisfied for n discritized elements.

- Strategy 1: a cathodic protection was applied in the tidal and splash zone and test area was painted every 15 years. This strategy was found to be considered when corrosion in the structure had initiated.
- Strategy 2: when 5% of the surface in splash and tidal zone shows minor signs of corrosion, the concrete was repaired and cathodic protection was applied.
- Strategy 3: when 30% of the surface in splash and tidal zone shows distinct corrosion damage, the complete exchange of concrete and reinforcement was done in corroded area.

The authors were found to carry out the deterministic and probabilistic optimization of three strategies. In each case the discount factor was found sensitive in decision making. However, the decision with preventive maintenance was found to be optimal.

Hawk (2003) studied Bridge Life Cycle Cost Analysis (BLCCA) methodologies and developed the software called BLCCA, in which the total life cycle cost (TLCC) was computed as the sum of total present value (PV) of all the costs anticipated during the service life .

$TLCC = PV\{[\ _{y\,c}\ CC(c,y)]- RV(T_A)\}$

where:

$CC(c,y)$ = cost of type c incurred in year y

$RV(T_A)$ = residual value at the end of the analysis period, $y = T_A$

y = sum over all years (y) in the analysis period

c = sum over all categories (c) of cost

PV = represent the equivalent value at the start of analysis, y = T_0

and,

$PV = FV_N / (1+DR)^N$

FV_N = future value of expenditure made at time N

N = number of time units between the present and future time

PV [CC] = PV[Agency Costs] + PV[Users Costs] + PV[Vulnerability Costs]

Agency costs were considered as the direct cost associated with the agency i.e. initial design and construction cost, inspection cost, maintenance cost, repair cost, rehabilitation cost and failure cost. The failure cost was the cost associated with failure multiplied by failure probability. User costs were the cost associated with the traffic delay, detours, accident due to the functional failure and the construction and maintenance activities on the bridge. The vulnerability costs were the cost associated with the natural hazards such as flooding, seismic events, or traffic occurrences and were found accounted in terms of probability of occurrence of such events.

6.2 Conclusion

The literature review in LCCA methods and strategies optimization, following conclusion can be made.

1. For alternatives having equal benefits, the LCCA can be done considering only the cost incurred throughout the service life of structures.

2. The performance measure is important while defining service life, and incorporating influence of maintenance and repair strategies. In practices, condition rating, safety, and reliability were found to be considered as performance indicator.
3. Probabilistic model can be considered while selecting alternatives. However, for the probabilistic model, input random variables and their distribution are necessary.
4. For the maintenance and repair decision, the criteria for the repair or repair threshold are important. These criteria might vary with bridge agency or bridge owners
5. Cost of failure is important parameter, and which depends on the actual scenario of failure and associated agency cost, users cost and other indirect costs. It is important to consider the failure probability in cost optimization to have idea on actual risk that the decision makers can holds in any repair and rehabilitation decisions.
6. User costs can be sensitive if comparable alternative strategies require traffic diversion, interruptions.
7. Discount rates are the important parameters and are to be considered for sensitivity study while making repair decisions

7 FRP COMPOSITE FOR CORROSION REPAIR

The use of fiber reinforced polymer (FRP) composites has been popular among the rehabilitation engineers as an alternative of the conventional repair materials. FRP composites are composed of carbon fibers, glass fibers, or aramid fibers that are embedded in a resin matrix which binds the fibers together. The FRP composites known to have very high strength-to-weight and stiffness-to-weight ratios as compared to traditional material like concrete and steel. Moreover, its fast construction, high durability, easy in handling and transportation, excellent fatigue and creep properties make it more popular. FRP composites have been widely used as an externally bonded reinforcement to repair and rehabilitation of existing structures to improve flexural, shear, axial compression and tension, and ductility of the RC structures.

The FRP composites system may vary depending on how they are delivered and installed in site. The commonly used FRP composite systems for the strengthening of structural members are wet layup systems, prepreg systems, precured system, and filament winding (ACI 440). The wet layup systems are widely used system and installation methods as it has flexibility in installation however it takes relatively higher installation time and found to have relatively lower quality as compared to other methods.

7.1 FRP in corrosion repair

Harichandran & Baiyasi (2000) carried out laboratory test and recommend wet lay-up method with the double layer Carbon/Epoxy or three layer Glass/Epoxy composites as method for repair of corrosion damaged Michigan bridge piers. Costs of repair were calculated to be $ 425/m2 and $ 360/m2 for Glass/Epoxy and Carbon/Epoxy composite repair. They didn't

consider cost benefit analysis to find cost effectiveness. New York State Department of Transportation (NYSDOT) also found to use double layer Carbon/Epoxy and three and five layer Glass/Epoxy FRP composites for the repair of damaged RC rectangular column (Halstead et al., 2000). The authors, based on the installation time, traffic interruption, and other effort, were found to recommend FRP composites as an effective means of bridge repair and rehabilitation.

From laboratory tests on wet-layup method of installation of Carbon/Epoxy or Glass/Epoxy composites it was found that they have shown acceptable performance to resist different environmental exposure condition, such as alkalinity, salt water, high temperature, humidity, chemical exposure, ultraviolet light, and freezing-and-thawing cycles (Zhang et al., 2002; Green et al.,2006; Khoe et al., 2011). Moreover, the use of CFRP and GFRP composites in repair of corroded RC structure was found to be effective to reduce the corrosion rate and to enhance strength, however in long-term, due to the radial expansion and internal cracking the loss in strength of substrate concrete was observed (Pantazopoulou et al. 2001; Debaiky et al., 2002; EI Maaddawy et al., 2006; Suh et al., 2007; Bae & Belarbi, 2009). In all works, the long-term performance profile of the composite along with substrate concrete was found unanswered.

7.2 Service life of repair

The service life of the FRP composites repair is important in optimizing the life-cycle cost. In practice, the ACI 440 recommended the durability parameters to be considered as suggested by manufacturers, with sufficient durability testing and as verified by the licensed professionals. ACI 440 further recommended the environmental reduction factor for different exposure condition, and for different fiber types. However, it doesn't account for the life of the repair. In TR-55, factor of safety were found to account the durability and material variability. It

further stated to use the service life of FRP strengthening work to be 30 years. Moreover, in both of the guidelines, the periodic inspection and maintenance is recommended.

Studies on the durability of FRP composites showed that the recommended ACI values are more conservatives in terms of strength reduction in long term (Karbhari & Abanilla, 2006). However, some recent study stated that the ACI 440 underestimate the environmental aging of FRP and epoxy in long term (Marouani et al., 2012). Moreover, considering risk of failure, the reliability study on the prediction of service life and LRFD design are being developed for FRP composite. NCHRP 665 recommends reliability index 3.5 for the externally bonded FRP design.

Hence it is recommended to use probabilistic reliability model to predict the service life of the repair/rehabilitation and optimize the LCCA based on probability of failure. The Arrhenius theory based strength deterioration curve for externally bonded FRP composites can be used to find the reliability as suggested by (Karbhari & Abanilla, 2006).

7.3 Service life of corroded RC structures

Chloride corrosion deterioration process is important to figure out the service life and to define the suitable time to carryout preventive maintenance, repair and rehabilitation in RC structures. The chloride corrosion deterioration process can be considered as shown in Figure 2. The time of corrosion initiation, time of corrosion cracking and end of functional service life of the structures depends on the chloride content, diffusion, concrete cover, concrete strength and maintenance strategies. For example, if we want to carry out preventive maintenance using sealers or coatings, it is good to apply before corrosion initiation during diffusion period. Once chloride threshold is reached, the preventive maintenance will not be effective, and hence concrete repair is needed.

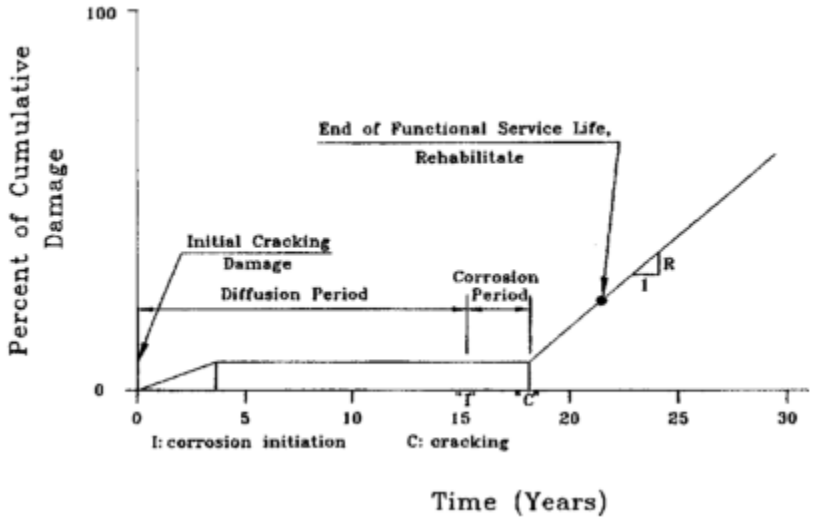

Figure 1. Chloride corrosion deterioration process for RC elements

Probabilistic model can be considered for the prediction of damage level in terms of corrosion initiation time using Fick's law and corrosion cracking time using any accepted model and hence corresponding probability distribution can be calculated for considered repair and rehabilitation strategies. However, statistical distribution of surface chloride content, diffusion coefficient, and concrete cover data are needed.

7.4 Corrosion repair strategies

The repair strategies depend on the institutional requirement and their standards. In general, following strategy is considered at this point of study. The threshold criteria and repair efficiency will be defined after DOT's survey.

1. Do noting
2. Use preventive maintenance and repair with FRP composite
3. Use preventive maintenance and rehabilitate with FRP composite.

These strategies will be optimized to achieve the best timing of repair. Use of number of layers, substrate repair quality, and type of FRP can be used in calculating reliability and failure probabilities to know the sensitivity on cost effectiveness.

8 LIFE-CYCLE COST ANALYSIS MODEL

For the study the LCCA model can be developed as explained, however it is subjected to change based on the information and data available. For the selected alternatives, the total life-cycle cost will be optimized to have minimum cost. The total cost is,

$$PV[C_t] = PV[\{C_i + C_m + C_{rep} \text{ or } C_{reh} + p_f \times C_f\} + C_{user}]$$

where,

C_t = total life-cycle cost

C_i = inspection cost

C_m = maintenance cost

C_{rep} = repair cost

C_{reh} = rehabilitation cost

C_f = failure cost

C_{user} = users cost

p_f = probability of failure of repaired/rehabilitated pier

PV = represent the equivalent value at the start of analysis

and,

$$PV = FV_N / (1+R)^N$$

FV_N = future value of expenditure made at time N

N = number of time units between the present and future time

R = prevailing discount rate

8.1 Cost of inspection and maintenance

The inspection is considered to be carried out every 2 years, and the preventive maintenance is considered to be carried out if required. At every 10 years interval, the substrate inspection is considered. It is considered as a unit cost per square ft of surface or per number of pier taken from prevailing DOTs practices or 0.1% of initial construction cost of pier per annum.

8.2 Cost of repair/rehabilitation

For the probability distribution of repair or rehabilitation, the method suggested by Engelund et al. (1999) and Mullard & Stewart (2012) can be considered and for the cost of repair can be calculated as suggested by Val & Stewart (2003).

$$C_{rep/reh}(T) = \sum_{i=1}^{T/\Delta t} \Delta p_{f,i} C_R$$

C_R can be calculated based on unit price costing of repair works i.e. $/sq.ft/layer. If the number of layers of FRP, its type, and area to be repaired is known then the cost of repair will be the sum of,

- Cost of material in $/sq.ft/layer [possible source; manufacturers]
- Cost of installation in $/sq.ft/layer [possible source; manufacturers]
- Cost of surface preparation in $/sq.ft/layer [possible source; DOTs]
- Cost of substrate repair and deep patching in $/sq.ft/layer (if substrate is repaired) [possible source; DOTs]

The requirement of substrate repair and its method is recommended to consider as per SHRP S-360.

8.3 Cost of failure

Cost of failure is the subject of optimization and it depends on the level of risk considered by the bridge owners. It can be calculated as the product of probability of failure during the service life of repair/ rehabilitation and the associated cost of failure. The probability of failure will depends on the type of the repair works, type of material, design thickness and other durability parameters.

8.4 Users cost

The user cost depends on the Average Annual Daily Traffic (AADT) of the specific route on which the considered bridge lies. Ehlen (1999) suggested the user cost as driver delay cost and vehicle operation cost described as,

$$Driver\ delay\ costs = \left(\frac{L}{S_a} - \frac{L}{S_n}\right) \times ADT \times N \times w$$

$$Vehicle\ operating\ costs = \left(\frac{L}{S_a} - \frac{L}{S_n}\right) \times ADT \times N \times r$$

where, L = length of affected roadway over which cars drive

S_a = traffic speed during road work

S_n = normal traffic speed

w = hourly time value of drivers

r = hourly vehicle operating cost

8.5 Price adjustment and discount rate

The time adjustment and the location adjustment can be done as per ENR price index and location index. The discount rate can be considered for the sensitivity study with 4%, 6% and 8% or any prevailing rates.

9 CONCLUSIONS

The Life-cycle cost analysis of the bridge pier can be done for the FRP composites which are known to have longer service life and fast in installation. The effectiveness of the timing of FRP application, type of repair material can be checked by probabilistic model using Monte-Carlo simulation. The long term durability of FRP composites, efficiency in corrosion control due to application of externally bonded FRP composites, time and spatial variation of corrosion parameters are the random variable and their statistical distribution are the key to use the proposed LCCA method. Moreover, the definition of threshold of repair is also important while selecting the decision of repair strategy.

10 REFERENCES

ACI Committee 440.2R-08 (2008). “Guide for the design and construction for externally bonded FRP systems for strengthening concrete structures.” American Concrete Institute, Michigan.

Andre´s A. Torres-Acosta and Miguel Martı´nez-Madrid, “Residual Life of Corroding Reinforced Concrete Structures in Marine Environment”, Journal of Materials in Civil Engineering, ISSN 0899-1561, 07/2003, Volume 15, Issue 4, pp. 344 – 353.

ASTM D2290-12 (2012). “Apparent Hoop Tensile Strength of Plastic or Reinforced Plastic Pipe” ASTM D3039/D3039M-14 (2014a). “Tensile Properties of Polymer Matrix Composite Materials”

ASTM A370-14 (2014b). “Standard Test Methods and Definitions for Mechanical Testing of Steel Products”

ASTM C39/C39M-14a (2014c). “Standard Test Method for Compressive Strength of Cylindrical Concrete Specimens”

Bae, S., and Belarbi, A. (2009). “Effect of corrosion of steel reinforcement on RC columns wrapped with FRP sheets.” *J. Perform.Constr. Facil.*, 23(1), 20-31.

Chen, Y., Davalos, J. F., Ray, I., and Kim, H. Y. (2007), “Accelerated aging tests for evaluation of durability performance of FRP reinforcing bars reinforcing bars for concrete structures.” Compos. Struct. 78(1), 101–111.

A

Debaiky, A.S., Green, M. F., and Hope, B.B. (2002). “Carbon fiber-reinforced polymer wraps for corrosion control and rehabilitation of reinforced concrete column.” *ACI Material Journal*., 99-M10.

Dong Chen, Sankaran Mahadevan, “Chloride-induced reinforcement corrosion and concrete cracking simulation”, Cement and Concrete Composites, ISSN 0958-9465, 2008, Volume 30, Issue 3, pp. 227 – 238.

Ehlen, M.A. (1999). “Life-cycle costs of fiber-reinforced-polymer bridge decks.” *J. Mater.Civ. Eng*., 11(3), 224-230.

Engelund, S., Sorensen, J. D., and Sorensen, B. (1999). “Evaluation of repair and maintenance strategies for concrete costal bridges on probabilistic basis.” *ACI Material Journal*., 96-M20.

EI Maadday, T., Chahrour, A., and Soudki, K. (2006). “Effect of fiber-reinforced polymer wraps on corrosion activity and concrete cracking in chloride-contaminated concrete cylinders.” *J. Comp. Const.*, 10(2), 139-147.

Fredrik P. Glasser, Jacques Marchand, Eric Samson, “Durability of concrete—Degradation phenomena involving detrimental chemical reactions”, Cement and Concrete Research, ISSN 008-8846, 2008, Volume 38, Issue 2, pp. 226 – 246.

Fam, A., Kong, A., and Green, M.(2008), “Effects of freezing and thawing cycles and sustained loading on compressive strength of precast concrete composite piles.”PCI J., 53(1), 109–120.

Frangopol, D. M., Lin, K. Y., and Estes, A. C. (1997). “Life – cycle cost design of deteriorating structures.” *J. Struct. Eng.*, 123(10), 1390-1401.

B

Halstead, J.P., Connor, J.S., Luu, K., Alampalli, S., and Minser, A. (2000). " Fiber-reinforced polymer wrapping of deteriorated concrete columns." *Transportation Research Record.,* 1696,142-130.

Harichandran, R. S., and Baiyasi, M. I. (2000). "Repair of corrosion-damaged columns using FRP wraps." *Research Report RC-1386,* Michigan Department of Transportation, MI.

Hawk, H. (2003). "Bridge life-cycle cost analysis." *National Cooperative Highway Research Program Report 483,* Transportation Research Board, Washington, D.C.

Green, M. F., Bisby, L. A., Fam, A. Z., and Kodur, V. K. R. (2006). "FRP confined concrte columns: Behavior under extreme conditions." *Cement & Concrete Composites.*, 28, 928-937.

Irina Stipanovic Oslakovic, Dubravka Bjegovic, Dunja Mikulic, "Evaluation of service life design models on concrete structures exposed to marine environment", Materials and Structures, ISSN 1359-5997, 12/2010, Volume 43, Issue 10, pp. 1397 – 1412.

Karbhari,V. M., and Abanilla, M. A. (2006). "Design factors, reliability, and durability prediction of wet layup carbon/epoxy used in external strengthening." *Composites. B.*, 38, 10-23.

Khoe, C., Sen, R., and Bhethanabotla, L. R. (2011). "Oxygen permeability of fiber-reinforced polymers." *J. Comp. Const.*, 15(4), 513-521.

Lin-Hai Han; Chao Hou; Qing-Li Wang (2012), "Square concrete filled steel tubular (CFST) members under loading and chloride corrosion: Experiments." Journal of Constructional Steel Research, 71, pg. 11-25.

Liu, M., and Frangopol, D. M. (2004). "Optimal bridge maintenance planning based on probabilistic performance prediction." *Eng. Struct.*, 26, 991-1002.

C

Marouani, S., Curtil, L., and Hamelin, P. (2012). “Ageing of carbon/epoxy and carbon/vinylester composites used in the reinforcement and/or the repair of civil engineering structures.” *Composites. B.*, 43, 2020-2030.

Mohammadi, J., Guralnick, S. A., and Yan, L. (1995). “Incorporating life-cycle costs in highway-bridge planning and design.” *J. Transp. Eng.*, 121(5), 417-424.

Mullard, J., and Stewart, M.G. (2012). “Life-cycle cost assessment of maintenance strategies for RC structures in chloride environment.” *J. Brdg. Eng.*, 17(2), 353-362.

Pantazopoulou, S. J., Bonacci, J. F., Sheikh, S., Thomas, M.D.A., and Hearn, N. (2001). “Repair of corrosion-damaged columns with FRP wraps.” *J. Comp. Const.*, 5(1), 0003-0011.

Stewart, M.G. (2001). “Reliability – based assessment of ageing bridges using risk ranking and lifecycle cost decision analyses.” *Reliab. Engg. Syst. Safe.*, 74, 263-273.

Suh, K., Mullins, G., Sen, R., and Winters, D. (2010). “Effective repair for corrosion control using FRP wraps.” *J. Comp. Const.*, 14(4), 388-396.

Robert, M. and Fam, A. (2012), “Long-Term Performance of GFRP Tubes Filled with Concrete and Subjected to Salt Solution.” J. Compos. Constr., 16(2), 217–224.

Shi, Xianming; Xie, Ning; Fortune, Keith; Gong, Jing, “Durability of steel reinforced concrete in chloride environments: An overview”, Construction and Building Materials, ISSN 0950-0618, 05/2012, Volume 30, Issue 1, pp. 125 – 138.

Seung-Woo Pack, Min-Sun Jung, Ha-Won Song, Sang-Hyo Kim, Ki Yong Ann, “Prediction of time dependent chloride transport in concrete structures exposed to a marine environment”, Cement and Concrete Research, ISSN 0008-8846, 2010, Volume 40, Issue 2, pp. 302 – 312.

D

Teng, J. G. , Yu, T. , and Wong, Y. L. (2004). “Behavior of hybrid FRP-concrete-steel double-skin tubular columns.” Proc., 2nd Int. Conf. on FRP Composites in Civil Engineering , Adelaide, Australia, 811–818

TR-55 (2000). “Design guide for strengthening concrete structures using fiber composite materials.” The Concrete Society, UK.

Val, D. V., and Stewart, M.G. (2003). “Life-cycle cost analysis of reinforced concrete structures in marine environments.” *Stru. Safe.*, 25, 343-362.

Zhang, J. S., Karbhari, V.M., Wu, L., and Reynaud, D. (2002). “Field exposure based durability assessment of FRP column wraps systems.” *Composites. B.*, 34, 41-50.

Zureick, A.H., Ellingwood, B.R., Nowak, A.S., Mertz, D.R., and Triantafillou, T.C. (2010). “Recommended guide specification for the design of externally bonded FRP systems for repair and strengthening of concrete bridge elements.” *NCHRP Report 665*, Transportation Research Board, Wasington, D.C.